Circulation: Arrhythmia and Electrophysiology

ORIGINAL ARTICLE

Atrial Fibrillation in Aging and Frail Mice

Modulation by Natriuretic Peptide Receptor C

Hailey J. Jansen, PhD; Motahareh Moghtadaei, PhD; Sara A. Rafferty, MSc; Robert A. Rose, PhD

BACKGROUND: Atrial fibrillation is prevalent in aging populations; however, not all individuals age at the same rate. Rather, health status during aging can vary from fit to frail. Frailty can be quantified using a frailty index (FI). Natriuretic peptides modulate atrial function in part by activating NP (natriuretic peptide) receptor C (NPR-C). The impacts of NPR-C on atrial structure and arrhythmogenesis in aging and as a function of frailty are unknown.

METHODS: Frailty was measured in aging wildtype and NPR-C knockout (NPR-C$^{-/-}$) mice. Atrial structure and function were studied using intracardiac electrophysiology in anesthetized mice, high-resolution optical mapping in intact atrial preparations, histology, and molecular biology.

RESULTS: NPR-C$^{-/-}$ mice had a shortened lifespan and more rapidly became frail compared with wildtype mice. Atrial fibrillation burden and P wave duration were increased in older versus younger wildtype mice and further increased in older NPR-C$^{-/-}$ mice; however, there was substantial variability among age groups and genotypes. P wave duration was strongly correlated with FI score regardless of age or genotype. Optical mapping of the atria demonstrated reduced conduction velocity and changes in action potential duration that were also graded by FI score. Atrial fibrosis was increased in aged and NPR-C$^{-/-}$ mice and was strongly correlated with FI score. Atrial fibrosis was associated with changes in expression of profibrotic genes, including MMPs (matrix metalloproteinases), TIMPs (tissue inhibitors of metalloproteinases), and TGFβ (transforming growth factor β). Gene expression changes were also correlated with FI scores.

CONCLUSIONS: NPR-C plays an essential role in the aging-dependent decline in health status as well as alterations in atrial function and arrhythmogenesis. Frailty assessment is a highly effective approach for identifying age-dependent heterogeneity in atrial structure and function, including in the setting of shortened lifespan because of loss of NPR-C.

GRAPHIC ABSTRACT: An online graphic abstract is available for this article.

Key Words: aging ■ atrial fibrillation ■ electrophysiology ■ fibrosis ■ frailty

Atrial fibrillation (AF), the most common sustained cardiac arrhythmia, is highly prevalent in aging populations.[1] Furthermore, progression of AF from paroxysmal forms to persistent or permanent AF is also associated with increasing age.[2] AF is associated with substantial morbidity and mortality because of increased risk of ischemic stroke, heart failure, and major impairments in quality of life.[3]

While age is clearly a critical risk factor for AF, not all individuals age in the same way or at the same rate. Rather, some individuals age more successfully, showing fewer health issues (ie, they are less frail), while others age more rapidly (ie, they are more frail).[4] As such, the health status of aging individuals can vary from fit to frail with more frail individuals being more susceptible to adverse health outcomes.[4] This heterogeneity in aging represents a major challenge for patient care including in AF.[5]

Frailty is thought to develop in association with the accumulation of health deficits over time.[4] Frailty can be quantified using a frailty index (FI) in which health status is assessed using well-established indicators of overall

Correspondence to: Robert A. Rose, PhD, Libin Cardiovascular Institute, Cumming School of Medicine, University of Calgary, GAC66, Health Research Innovation Centre, 3280 Hospital Drive NW, Calgary, Alberta, Canada T2N 4Z6. Email robert.rose@ucalgary.ca
The Data Supplement is available at https://www.ahajournals.org/doi/suppl/10.1161/CIRCEP.121.010077.
For Sources of Funding and Disclosures, see page 872.

Circulation: Arrhythmia and Electrophysiology is available at www.ahajournals.org/journal/circep

WHAT IS KNOWN?

- Atrial fibrillation is prevalent in aging and can occur in association with alterations in atrial conduction and atrial fibrosis.
- Natriuretic peptides can act upon natriuretic peptide receptor C to modulate atrial structure and function.

WHAT THE STUDY ADDS

- Loss of natriuretic peptide receptor C results in shorted lifespan in association with the development of frailty.
- Atrial electrical function declines with age in wildtype and natriuretic peptide receptor C knockout mice; however, differences were more effectively identified as a function of frailty (ie, health status) than chronological age.
- Frailty assessment is an effective approach for identifying age-dependent heterogeneity in atrial structure and function including in the setting of altered natriuretic peptide receptor C signaling.

Nonstandard Abbreviations and Acronyms

AF	atrial fibrillation
ANP	atrial natriuretic peptide
AP	action potential
APD	action potential duration
CNP	C-type natriuretic peptide
CV	conduction velocity
FI	frailty index
LA	left atrial
MMP	matrix metalloproteinase
NP	natriuretic peptide
NPR-C	natriuretic peptide receptor C
NPR-C$^{-/-}$	natriuretic peptide receptor C knockout
RA	right atrial
TIMP	tissue inhibitor of metalloproteinase
WT	wildtype

health.[4,6] We recently developed a noninvasive clinical FI for use in mice based on the assessment of 31 indicators of health status.[7] This FI uses 31 readily apparent, well-established signs of clinical deterioration in overall health status. In this approach, the FI score for an individual is determined by quantifying the number of deficits present and dividing by the total number of items measured to generate a score between 0 (no deficits present, least frail) and 1 (all deficits present, most frail). The mouse clinical FI is based on similar approaches used in human patients and has been shown to very accurately reproduce the main features of deficit accumulation and frailty development in aging humans.[4,7] We have previously shown that the mouse clinical FI can effectively distinguish differences in health status and identify frailty-dependent changes in cardiac function, including atrial remodeling, in aging mice.[8–10]

NPs (natriuretic peptides) are a family of cardioprotective hormones that play critical roles in regulating cardiac structure and cardiac electrophysiology.[11,12] Interestingly, studies have shown that circulating levels of ANP (atrial natriuretic peptide) and CNP (C-type natriuretic peptide) decline in aging rats, and that this is associated with enhanced cardiac fibrosis,[13,14] suggesting that derangements in the NP system can contribute importantly to aging-related cardiac dysfunction.

NPs elicit their effects in part by activating NP receptor C (NPR-C), which has high affinity for all NPs.[12] NPR-C is highly expressed in the atria and has previously been shown to regulate atrial electrophysiology and susceptibility to AF.[15–17] However, the role of NPR-C in aging-related changes in atrial electrophysiology and arrhythmogenesis are unknown. Also, whether NPR-C affects frailty development in aging mice has not been investigated. Accordingly, the purpose of this study was to assess atrial arrhythmogenesis, atrial electrophysiology, and atrial fibrosis in wildtype (WT) and NPR-C knockout (NPR-C$^{-/-}$) mice as a function of age and frailty.

METHODS

An expanded methods section is available in the Methods in the Data Supplement. All data and materials used in this study are available upon reasonable request to the corresponding author.

Mice

This study used male and female WT and NPR-C$^{-/-}$ mice. All experimental procedures were approved by the University of Calgary Animal Care and Use Committee or the Dalhousie University Committee for Laboratory Animals and conformed to the guidelines of the Canadian Council on Animal Care.

Frailty Assessment

Frailty was assessed in all mice using our noninvasive 31 item frailty index as described previously[7–9] and in Methods in the Data Supplement.

In Vivo Electrophysiology and Programmed Stimulation

ECG intervals and AF susceptibility were measured in anesthetized mice using intracardiac programmed stimulation as described previously[16,18] and in Methods in the Data Supplement.

High-Resolution Optical Mapping

Activation patterns and electrical conduction in the atria were investigated using high-resolution optical mapping in isolated atrial preparations as described previously[16,19] and in Methods in the Data Supplement.

Histology

Interstitial collagen was assessed by picrosirius red staining as previously described.[16,19]

Quantitative PCR

Gene expression was measured in the right and left atria as described previously[16,19] and in Methods in the Data Supplement.

Statistical Analysis

Data are presented as mean±SEM. Data were analyzed using the Fisher exact test, 1-way ANOVA with a Tukey posthoc test, or 2-way ANOVA with a Tukey posthoc test as indicated in each figure legend. To assess differences as a function of FI score linear regression analysis was used to obtain Pearson correlations. In all cases, $P<0.05$ was considered significant.

RESULTS

Survival and Frailty in Aging WT and NPR-C$^{-/-}$ Mice

To determine the impacts of NPR-C on lifespan and health status during aging FI scores were measured in WT and NPR-C$^{-/-}$ mice beginning at 20 weeks of age (Figure 1). WT mice were aged up to 110 weeks during which FI scores increased.[7,9] FI scores in NPR-C$^{-/-}$ mice were higher than WT mice at all time points assessed (Figure 1A). Strikingly, NPR-C$^{-/-}$ mice reached maximum FI scores (ie, health status declined) much earlier than WT mice. The majority of NPR-C$^{-/-}$ mice died or had to be euthanized for humane reasons by 70 weeks of age. Consistent with this, 1-year survival curves demonstrate that NPR-C$^{-/-}$ mice have reduced survival compared with WT mice (Figure 1B). These data indicate that loss of NPR-C results in shortened lifespan in association with a more rapid development of frailty.

To investigate how the loss of NPR-C affects atrial function during aging, we investigated younger (≈20 weeks of age) and older (≈60 weeks of age) cohorts of male and female WT and NPR-C$^{-/-}$ mice (Figure 1C). On average, FI scores were higher in older versus younger mice and in NPR-C$^{-/-}$ compared with WT mice (Figure 1D). It should also be noted that there is a range of FI scores within each group and that these values can overlap, which is indicative of differences in health status regardless of chronological age or genotype. Ages and FI scores were similar between male and female WT and NPR-C$^{-/-}$ mice (Figure II in the Data Supplement).

AF and Atrial Electrophysiology in Aging WT and NPR-C$^{-/-}$ Mice

Younger NPR-C$^{-/-}$ mice had increased susceptibility to burst pacing induced AF compared with younger WT mice (Figure 2A and 2B). There were also trends ($P=0.066$) toward increased susceptibility to AF in older NPR-C$^{-/-}$ mice compared with older WT mice (Figure 2B). AF durations where often longer in younger and older NPR-C$^{-/-}$ mice compared with WT mice (Figure 2C). AF was also assessed as a function of FI score in the same mice as presented in Figure 2B and 2C. These data demonstrate that AF inducibility was increased and AF duration was longer at higher FI scores (Figure 2D and 2E).

Surface ECGs (Figure 3A and 3B) demonstrate that P wave duration was increased in older versus younger WT mice (Figure 3C) and in NPR-C$^{-/-}$ mice compared with WT mice at both ages; however, differences in P wave

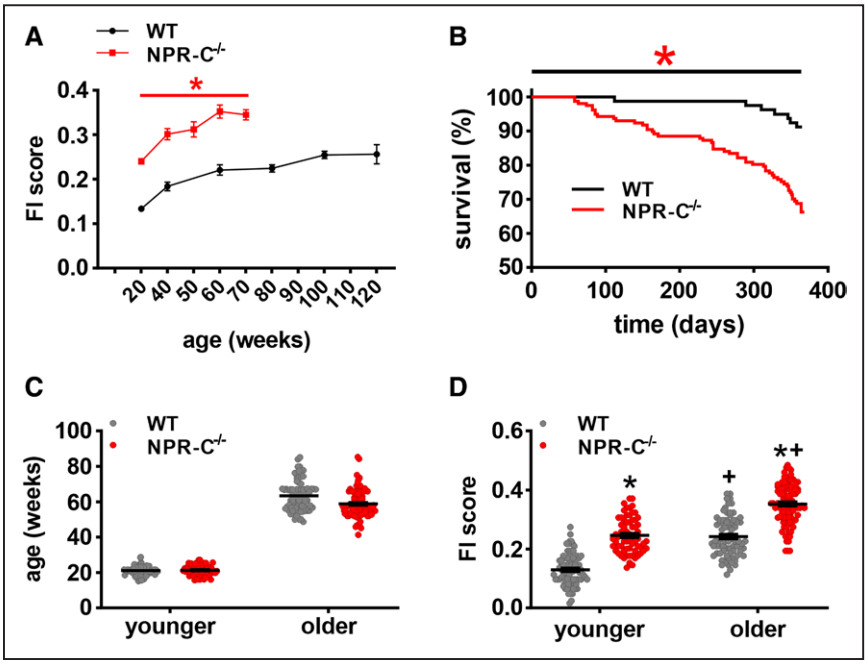

Figure 1. Frailty and survival in aging NPR-C$^{-/-}$ mice.
A, Changes in Frailty index (FI) score in aging WT and NPR-C$^{-/-}$ mice. *$P<0.05$ vs WT by 2-way repeated measures ANOVA. **B**, 1 y survival curve for WT ($n=79$) and NPR-C$^{-/-}$ ($n=157$) mice. *$P<0.05$ vs WT by Log-rank test. **C**, Ages of younger and older WT and NPR-C$^{-/-}$ mice used to evaluate atrial function in this study. **D**, FI scores in younger and older WT and NPR-C$^{-/-}$ mice (same mice as [**A**]). *$P<0.05$ vs WT; +$P<0.05$ vs younger by 2-way ANOVA with a Tukey posthoc test. **C** and **D**, $n=85$ for WT-younger, 76 for WT-older, 66 for NPR-C$^{-/-}$-younger, and 95 for NPR-C$^{-/-}$-older.

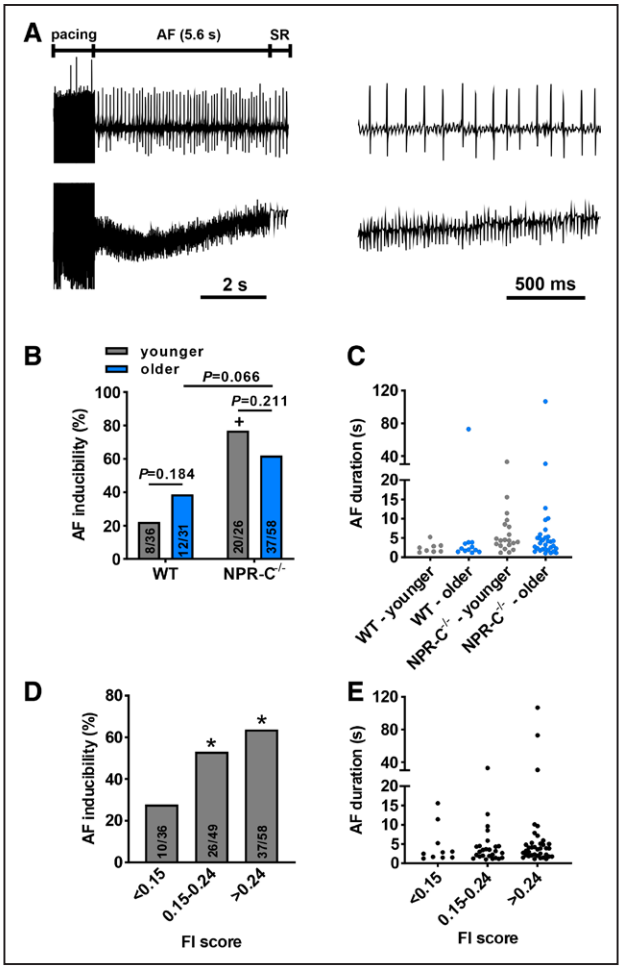

Figure 2. Susceptibility to atrial fibrillation in younger and older wild-type (WT) and NPR-C$^{-/-}$ mice.
A, Representative surface ECG (top) and intracardiac atrial electrogram (bottom) showing the induction of atrial fibrillation (AF) after burst pacing and the reversion back to sinus rhythm (SR). Recordings on the right illustrate magnified view of surface ECG and atrial electrograms during AF. **B**, Inducibility of AF in younger and older WT and NPR-C$^{-/-}$ mice. Numbers in bars indicate the number of mice induced into AF. +P<0.05 vs WT at same age. Data analyzed by Fisher exact test. **C**, Duration of AF when induced in younger and older WT and NPR-C$^{-/-}$ mice. **D**, Inducibility of AF in all younger and older WT and NPR-C$^{-/-}$ mice (same mice as presented in **B**) as a function of FI score. *P<0.05 vs the <0.15 FI score bin by Fisher exact test. **E**, Duration of AF in the same mice as presented in **D** as a function of FI score.

duration were not detected when comparing younger and older NPR-C$^{-/-}$ mice (Figure 3C). Notably, there was variability in P wave duration within each age group and genotype, particularly in aged NPR-C$^{-/-}$ mice, suggesting that factors other than chronological age could impact atrial electrophysiology. Accordingly, P wave duration in all younger and older WT and NPR-C$^{-/-}$ mice was plotted as a function of FI score (Figure 3D). These data demonstrate that P wave duration is strongly correlated with FI score and that mice with similar FI scores have similar P wave durations regardless of chronological age or genotype. Changes in P wave duration as a function of chronological age and FI score were similar between male and female WT and NPR-C$^{-/-}$ mice (Figure III in the Data Supplement).

PR interval was increased in older versus younger mice and in NPR-C$^{-/-}$ versus WT mice (Figure 3E). Once again, there was substantial variability in each group of mice; however, measuring PR interval as function of frailty demonstrates that PR interval is strongly correlated with FI score (Figure 3F). These changes in PR interval were similar between male and female WT and NPR-C$^{-/-}$ mice (Figure IV in the Data Supplement). As sex differences were not apparent in these atrial electrophysiology studies, male and female data were combined in subsequent figures.

Atrial Conduction and AP Morphology in Aging WT and NPR-C$^{-/-}$ Mice

High-resolution optical mapping in isolated atrial preparations from younger and older WT and NPR-C$^{-/-}$ mice (Figure 4A) demonstrate that right atrial (RA) conduction velocity (CV) was reduced in older versus younger WT mice and in younger NPR-C$^{-/-}$ versus younger WT mice (Figure 4B). RA CV also tended to be lower (P=0.078) in older NPR-C$^{-/-}$ compared with younger NPR-C$^{-/-}$ mice (Figure 4B). No differences in RA CV were observed between older WT and older NPR-C$^{-/-}$ mice, which showed variability within each group. Nevertheless, when measured as a function of frailty, RA CV exhibited a strong negative correlation with FI score (Figure 4C). Similar patterns were seen for left atrial (LA) conduction velocity (Figure 4D and 4E).

Optical APs from the right and left atria were used to assess AP duration (APD) in younger and older WT and NPR-C$^{-/-}$ mice (Figure 5A). RA APD_{50} and APD_{90} were shorter in older versus younger mice in both genotypes; however, APD was not different between WT and NPR-C$^{-/-}$ mice within age groups (Figure 5B and 5C). When measured as a function of frailty, RA APD_{50} and APD_{90} were negatively correlated with FI score such that APDs were shorter at higher FI scores (Figure 5D and 5E). Similar patterns were observed for LA APD_{50} and APD_{90} as a function of chronological age (Figure 5F and 5G) and as a function of FI score (Figure 5H and 5I).

The wavelength of reentry, which is the product of CV and the effective refractory period,[3,20] was estimated in optical mapping studies as the product of CV and APD_{90} (Figure V in the Data Supplement). In the right atrium, wavelength was reduced in older versus younger mice and in younger NPR-C$^{-/-}$ mice compared with younger WT mice; however, differences were not detected between older NPR-C$^{-/-}$ mice and older WT mice (Figure V in the Data Supplement). Nevertheless, wavelength showed a strong negative correlation with FI score in the right atrium (Figure V in the Data Supplement). Similar patterns were observed in the left atrium as a function of

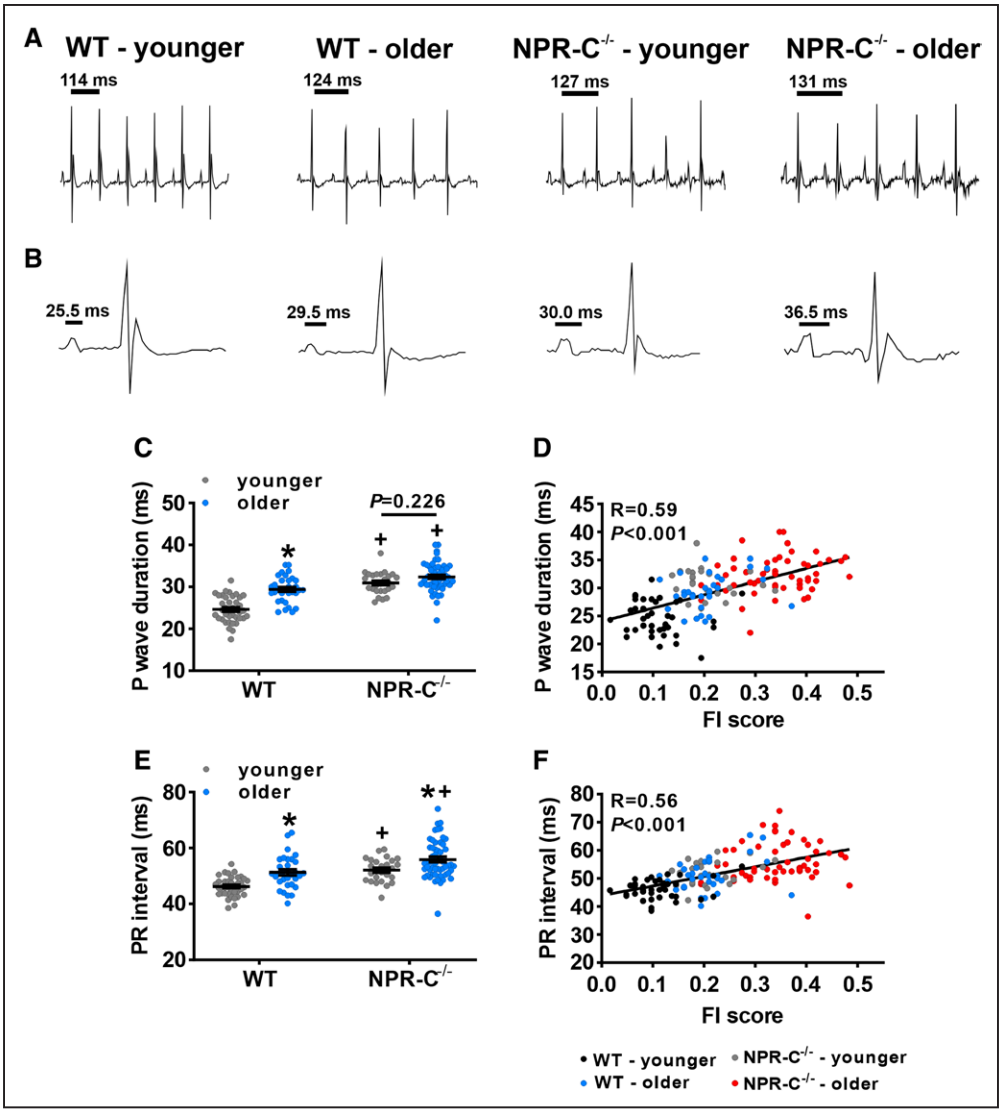

Figure 3. Effects of age and frailty on atrial electrophysiology in wild-type (WT) and NPR-C$^{-/-}$ mice in vivo.
A, Representative surface ECGs in younger and older WT and NPR-C$^{-/-}$ mice. Bars indicate RR intervals in each example. **B**, Representative single ECG beats in younger and older WT and NPR-C$^{-/-}$ mice. Bars indicate P wave duration in each example. **C**, P wave duration in younger and older WT and NPR-C$^{-/-}$ mice (males and females combined). *P<0.05 vs younger; +P<0.05 vs WT by 2-way ANOVA with a Tukey posthoc test. **D**, P wave duration as a function of FI score for younger and older WT and NPR-C$^{-/-}$ mice (same mice as **C**). Linear regression analyzed using Pearson correlation. **E**, PR interval in younger and older WT and NPR-C$^{-/-}$ mice. *P<0.05 vs younger; +P<0.05 vs WT by 2-way ANOVA with a Tukey posthoc test. **F**, PR interval as a function of FI score for younger and older WT and NPR-C$^{-/-}$ mice (same mice as **E**). Linear regression analyzed using Pearson correlation. n=38 mice for WT-younger, 32 for WT-older, 26 for NPR-C$^{-/-}$-younger, and 53 for NPR-C$^{-/-}$-older.

age and genotype and as a function of FI score (Figure V in the Data Supplement).

Atrial Fibrosis in Aging WT and NPR-C$^{-/-}$ Mice

RA and LA fibrosis was assessed histologically in younger and older WT and NPR-C$^{-/-}$ mice (Figure 6A). In the right atrium, interstitial fibrosis was increased in older versus younger WT and NPR-C$^{-/-}$ mice (Figure 6B). RA interstitial fibrosis was also increased in younger NPR-C$^{-/-}$ compared with younger WT mice (Figure 6B). Conversely, no differences were observed between older NPR-C$^{-/-}$ compared with older WT mice (Figure 6B). Frailty analysis demonstrates that RA interstitial fibrosis was strongly correlated with FI score (Figure 6C). In the left atrium, interstitial fibrosis was increased in younger versus older and NPR-C$^{-/-}$ versus WT mice (Figure 6D). Once again, LA fibrosis was strongly correlated with FI score (Figure 6E).

Next, the expression of genes involved in atrial conduction velocity and fibrosis were measured. Atrial CV is importantly affected by the Na^+ channel, encoded by the *scn5a* gene. *Scn5a* expression was not altered in the RA (Figure 7A). In the LA, *scn5a* expression was reduced in NPR-C$^{-/-}$ mice compared with WT mice; however, differences were not detected between older

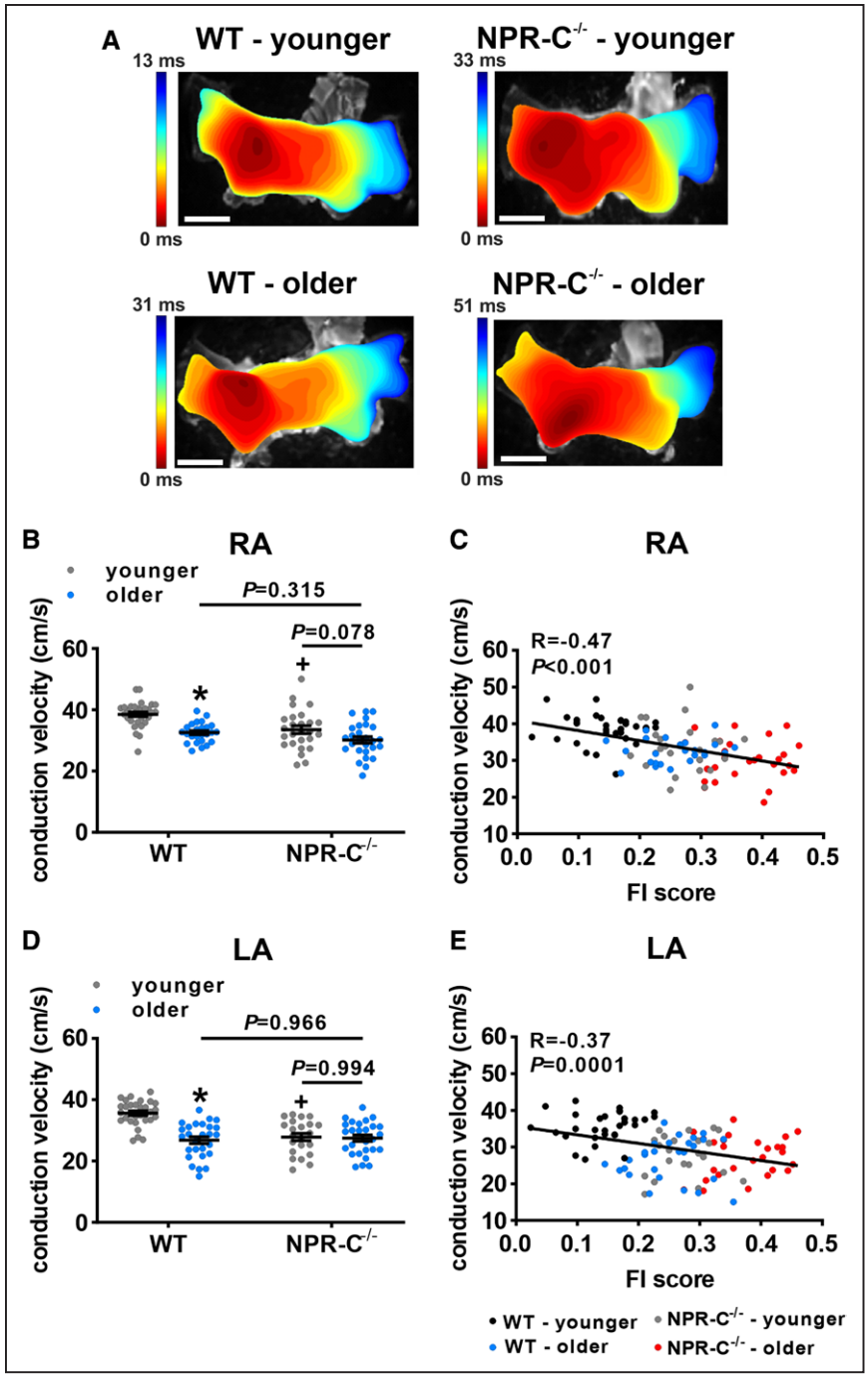

Figure 4. Effects of age and frailty on atrial electrical conduction in wild-type (WT) and NPR-C$^{-/-}$ mice. **A**, Representative activation maps in younger and older WT and NPR-C$^{-/-}$ mice. Right atrium is on the left side of the images. Red color indicates earliest activation time. Scale bars are 2 mm. **B**, Right atrial (RA) conduction velocity in younger and older WT and NPR-C$^{-/-}$ mice. *P<0.05 vs younger; +P<0.05 vs WT by 2-way ANOVA with a Tukey posthoc test. **C**, RA conduction velocity as a function of frailty index (FI) score for younger and older WT and NPR-C$^{-/-}$ mice (same mice as **B**). Linear regression analyzed using Pearson correlation. **B** and **C**, n=30 mice for WT-younger, 25 for WT-older, 26 for NPR-C$^{-/-}$-younger, and 27 for NPR-C$^{-/-}$-older. **D**, Left atrial (LA) conduction velocity in younger and older WT and NPR-C$^{-/-}$ mice. *P<0.05 vs younger; +P<0.05 vs WT by 2-way ANOVA with a Tukey posthoc test. **C**, LA conduction velocity as a function of FI score for younger and older WT and NPR-C$^{-/-}$ mice (same mice as **D**). Linear regression analyzed using Pearson correlation. **D** and **E**, n=30 mice for WT-younger, 27 for WT-older, 22 for NPR-C$^{-/-}$-younger, and 27 for NPR-C$^{-/-}$-older.

and younger mice (Figure 7B). Nevertheless, *scn5a* expression was negatively correlated with FI score in the LA (Figure 7B).

RA expression of *col1a* (encodes collagen type I) was not different in older versus younger WT mice and was modestly reduced in older versus younger NPR-C$^{-/-}$ mice (Figure 7C). No differences were observed in *col1a* expression as a function of chronological age in the LA in WT and NPR-C$^{-/-}$ mice (Figure 7D). When measured as a function of frailty, *col1a* expression was positively correlated with FI score in the left atrium, but not the RA (Figure 7C and 7D). No differences in expression of *col3a* (encodes collagen type III) were observed in the right or left atria as function of age or FI score (Figure VI in the Data Supplement).

RA expression of *tgfb1* (encodes TGFβ) was increased in younger and older NPR-C$^{-/-}$ mice compared with WT mice (Figure 7E). RA *tbgb1* expression was also increased in older versus younger NPR-C$^{-/-}$ mice (Figure 7E). In addition, RA expression of *tgfb1* was correlated with FI score (Figure 7E). No differences were observed in LA *tgfb1* expression (Figure 7F).

Right and LA expression of *mmp2* (encodes MMP2 [matrix metalloproteinase 2]) was variable when

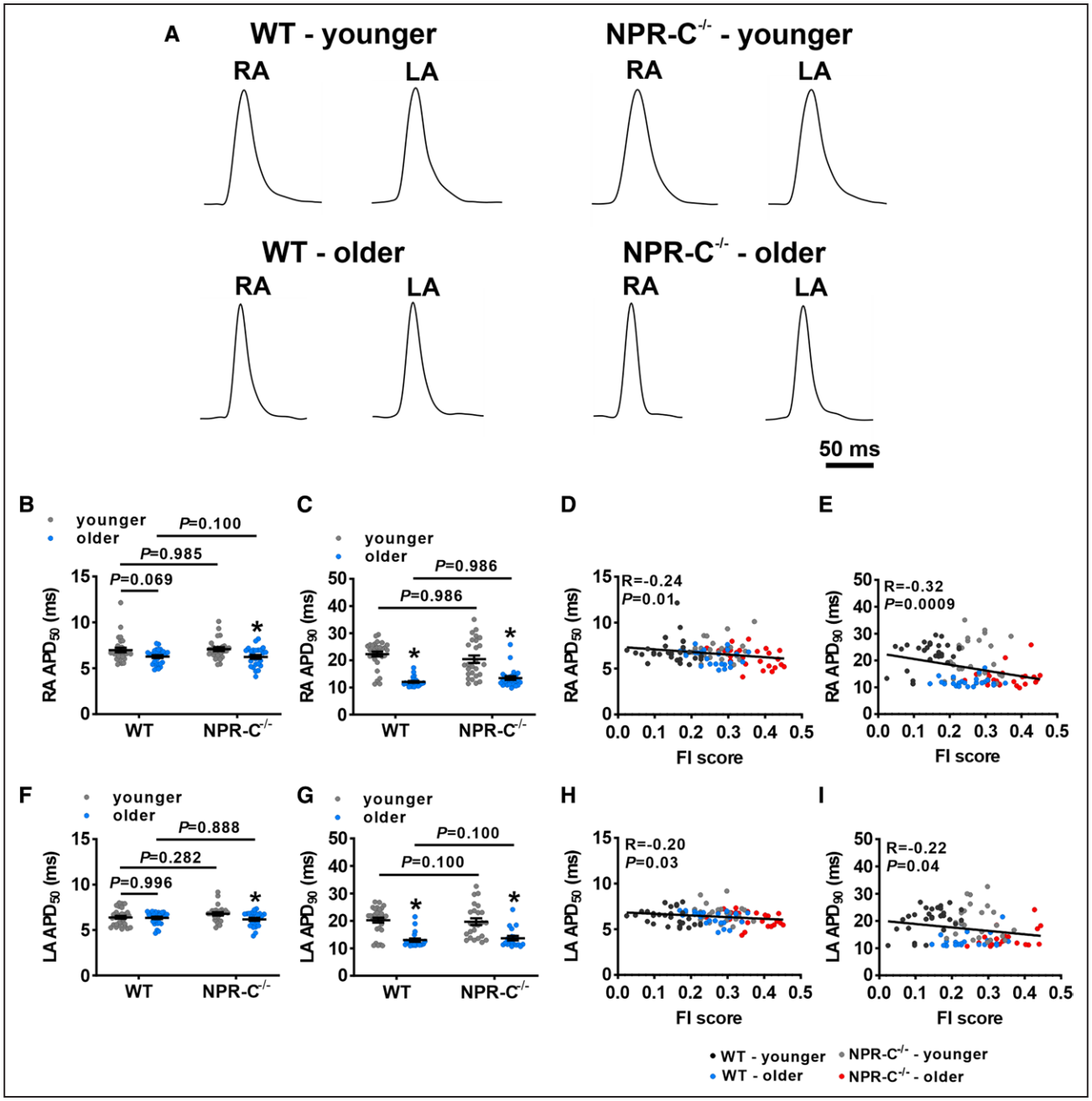

Figure 5. Effects of age and frailty on atrial action potential morphology in wild-type (WT) and NPR-C$^{-/-}$ mice.
A, Representative right atrial (RA) and left atrial (LA) optical action potentials (APs) from younger and older WT and NPR-C$^{-/-}$ mice. **B**, RA APD_{50} in younger and older WT and NPR-C$^{-/-}$ mice. *n*=30 for WT-younger, 28 for WT-older, 26 for NPR-C$^{-/-}$-younger, and 26 for NPR-C$^{-/-}$-older. **C**, RA APD_{90} in younger and older WT and NPR-C$^{-/-}$ mice. *n*=30 for WT-younger, 25 for WT-older, 26 for NPR-C$^{-/-}$-younger, and 25 for NPR-C$^{-/-}$-older. **B** and **C**, **P*<0.05 vs younger by 2-way ANOVA with a Tukey posthoc test. **D** and **E**, RA APD_{50} (**D**) and APD_{90} (**E**) as a function of frailty index (FI) score in younger and older WT and NPR-C$^{-/-}$ mice (same mice as **B** and **C**). Linear regressions analyzed using Pearson correlation. **F**, LA APD_{50} in younger and older WT and NPR-C$^{-/-}$ mice. *n*=31 for WT-younger, 28 for WT-older, 25 for NPR-C$^{-/-}$-younger, and 26 for NPR-C$^{-/-}$-older. **G**, LA APD_{90} in younger and older WT and NPR-C$^{-/-}$ mice. *n*=30 for WT-younger, 22 for WT-older, 22 for NPR-C$^{-/-}$-younger, and 19 for NPR-C$^{-/-}$-older. **F** and **G**, **P*<0.05 vs younger by 2-way ANOVA with a Tukey posthoc test. **H** and **I**, LA APD_{50} (**H**) and APD_{90} (**I**) as a function of FI score in younger and older WT and NPR-C$^{-/-}$ mice (same mice as **F** and **G**). Linear regressions analyzed using Pearson correlation.

measured as a function of age in WT and NPR-C$^{-/-}$ but was increased in younger NPR-C$^{-/-}$ mice versus younger WT mice in the RA and reduced in older WT mice versus younger WT mice in the LA (Figure 8A and 8B). When measured as function of frailty, RA *mmp2* expression was positively correlated with FI score while LA *mmp2* expression was negatively correlated with FI score (Figure 8A and 8B). RA expression of *mmp9* (encodes MMP9) was increased in older versus younger NPR-C$^{-/-}$ mice but was otherwise unchanged when

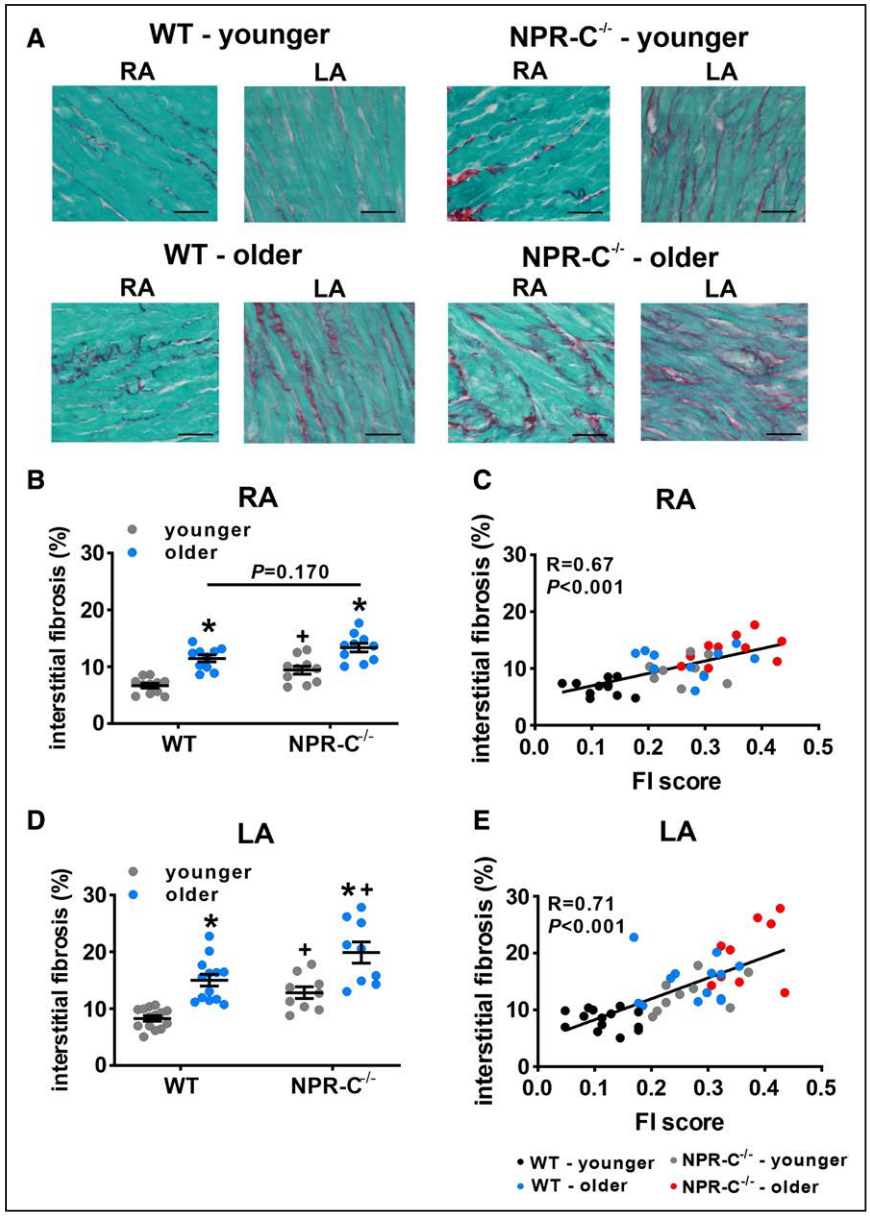

Figure 6. Effects of age and frailty on atrial fibrosis in wild-type (WT) and NPR-C$^{-/-}$ mice.
A, Representative images demonstrating patterns of interstitial collagen (shown in red) in the right atrium (RA) and left atrium (LA) in younger and older WT and NPR-C$^{-/-}$ mice. Scale bar is 50 μm. **B**, RA interstitial fibrosis in younger and older WT and NPR-C$^{-/-}$ mice. *n*=11 for WT-younger, 10 for WT-older, 10 for NPR-C$^{-/-}$-younger, and 10 for NPR-C$^{-/-}$-older. **P*<0.05 vs younger; +*P*<0.05 vs WT by 2-way ANOVA with a Tukey posthoc test. **C**, RA interstitial fibrosis in younger and older WT and NPR-C$^{-/-}$ mice as a function of FI score (same mice as **B**). Linear regression analyzed using Pearson correlation. **D**, LA interstitial fibrosis in younger and older WT and NPR-C$^{-/-}$ mice. *n*=14 for WT-younger, 13 for WT-older, 9 for NPR-C$^{-/-}$-younger, and 9 for NPR-C$^{-/-}$-older. **P*<0.05 vs younger; +*P*<0.05 vs WT by 2-way ANOVA with a Tukey posthoc test. **E**, LA interstitial fibrosis in younger and older WT and NPR-C$^{-/-}$ mice as a function of FI score (same mice as **D**). Linear regression analyzed using Pearson correlation.

measured as a function of age or FI score in the right and left atria (Figure 8C and 8D).

Next, expression of TIMPs (tissue inhibitors of metalloproteinases) was assessed. RA expression of *timp1* was increased in older versus younger WT mice and in younger NPR-C$^{-/-}$ mice versus younger WT mice (Figure 8E), while LA expression of *timp1* was increased in older versus younger NPR-C$^{-/-}$ mice (Figure 8F). In addition, *timp1* expression showed a clear trend for a positive correlation with FI score in the right atrium (Figure 8E) and was also positively correlated with FI score in the left atrium (Figure 8F). As remodeling of the extracellular matrix is affected by the balance between TIMP and MMP activity, the ratio of *timp1* expression to the expression of *mmp2* and *mmp9* was also quantified (Figure VII in the Data Supplement). These data show that *timp1/mmp2* in the LA and *timp1/mmp9* in the right and left atria were all correlated with FI score. RA and LA expression of *timp2*, *timp3,* and *timp4* was more variable, but some regional expression changes were observed. For example, frailty analysis identified negative correlations with FI score for *timp3* in the right atrium and *timp4* in the left atrium (Figure VIII in the Data Supplement).

DISCUSSION

This study demonstrates that loss of NPR-C substantially shortens the lifespan of mice in association with more rapid development of frailty. While WT mice can live for ≈130 weeks (ie, ≈2.5 years),[7] no NPR-C$^{-/-}$ mice survived past ≈80 weeks of age (corresponds to ≈50 years of age in humans). FI scores were higher in NPR-C$^{-/-}$ mice at all time points measured and reached maximum values at ≈70 to 80 weeks of age. The mouse clinical FI

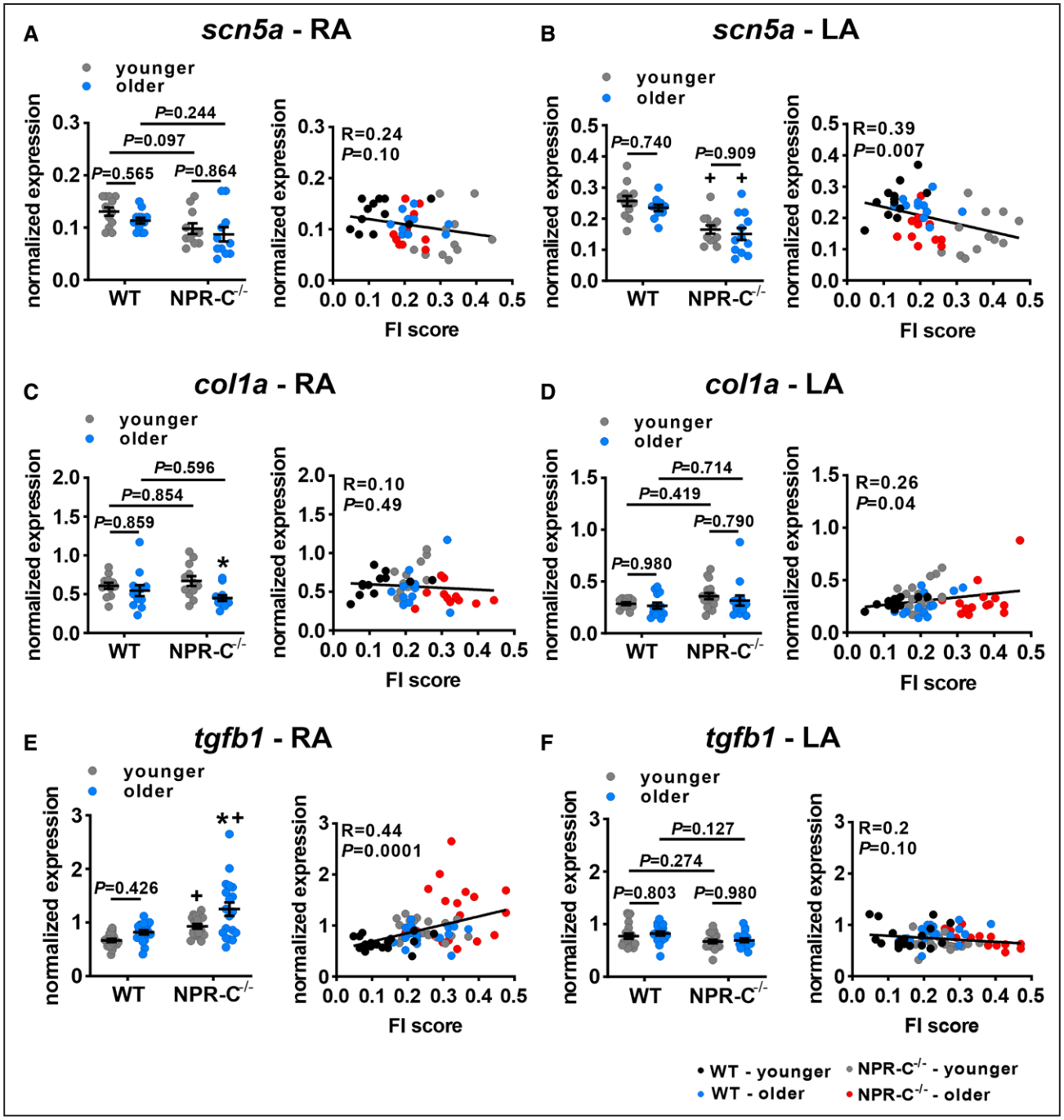

Figure 7. Expression of scn5a, collagen type I and transforming growth factor β in the atria of wild-type (WT) and NPR-C$^{-/-}$ mice. **A**, Right atrial (RA) expression of *scn5a* mRNA in younger and older WT and NPR-C$^{-/-}$ mice (left) and as a function of FI score (right). *n*=12 for WT-younger, 12 for WT-older, 11 for NPR-C$^{-/-}$-younger, and 11 for NPR-C$^{-/-}$-older. **B**, Left atrial (LA) expression of *scn5a* mRNA in younger and older WT and NPR-C$^{-/-}$ mice (left) and as a function of frailty index (FI) score (right). *n*=12 for WT-younger, 11 for WT-older, 12 for NPR-C$^{-/-}$-younger, and 12 for NPR-C$^{-/-}$-older. **C**, RA *col1a* mRNA expression in younger and older WT and NPR-C$^{-/-}$ mice (left) and as a function of FI score (right). *n*=12 for WT-younger, 12 for WT-older, 12 for NPR-C$^{-/-}$-younger, and 12 for NPR-C$^{-/-}$-older. **D**, LA *col1a* mRNA expression in younger and older WT and NPR-C$^{-/-}$ mice (left) and as a function of FI score (right). *n*=12 for WT-younger, 14 for WT-older, 17 for NPR-C$^{-/-}$-younger, and 14 for NPR-C$^{-/-}$-older. **E**, RA *tgfb1* mRNA expression in younger and older WT and NPR-C$^{-/-}$ mice (left) and as a function of FI score (right). *n*=19 for WT-younger, 20 for WT-older, 19 for NPR-C$^{-/-}$-younger, and 19 for NPR-C$^{-/-}$-older. **F**, LA *tgfb1* mRNA expression in younger and older WT and NPR-C$^{-/-}$ mice (left) and as a function of FI score (right). *n*=20 for WT-younger, 19 for WT-older, 19 for NPR-C$^{-/-}$-younger, and 17 for NPR-C$^{-/-}$-older. For figures as a function of chronological age *P<0.05 vs younger; +P<0.05 vs WT by 2-way ANOVA with a Tukey posthoc test. For figures as a function of FI score linear regressions analyzed using Pearson correlation.

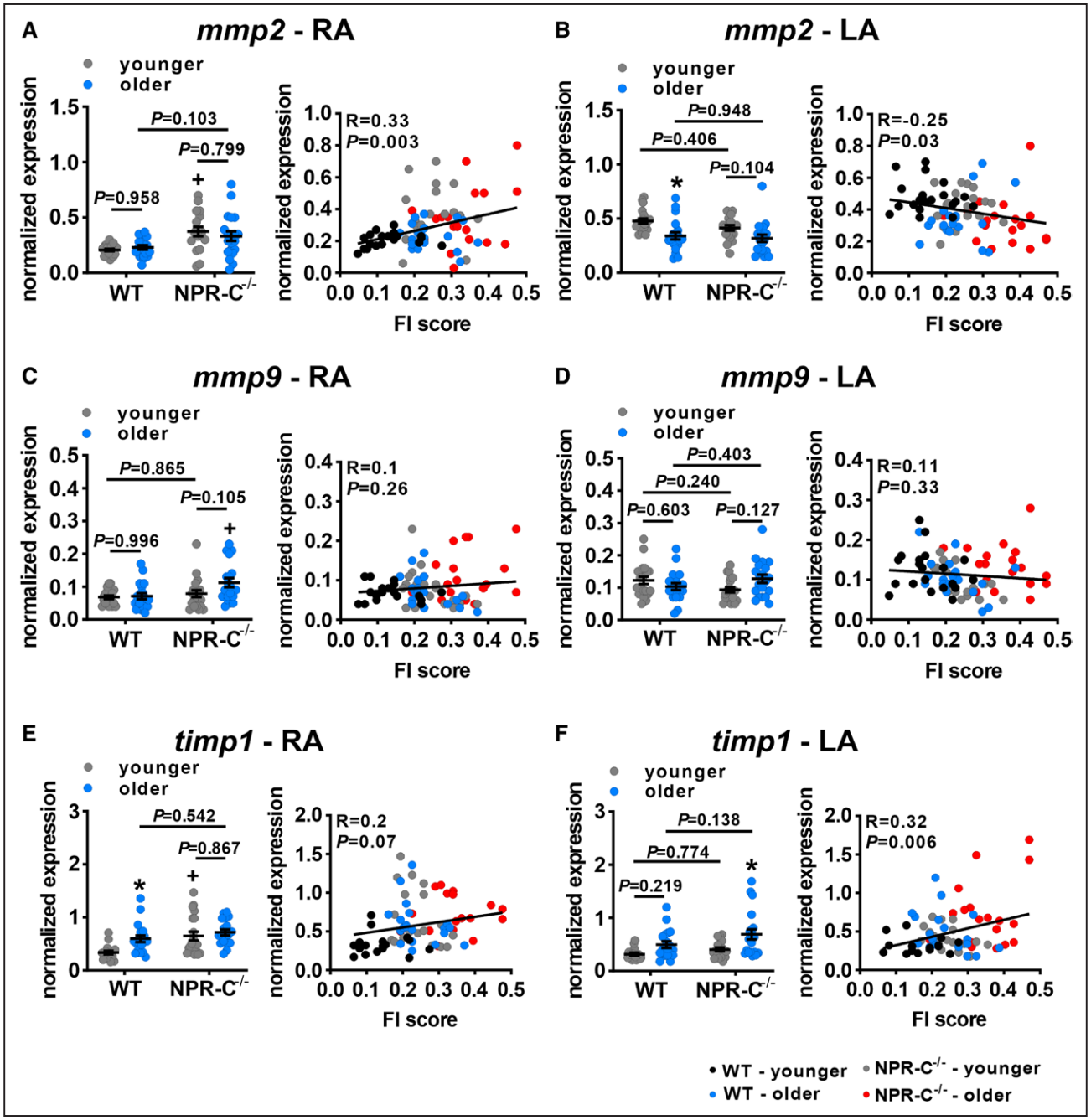

Figure 8. Expression of matrix metalloproteinase 2, matrix metalloproteinase 9, and tissue inhibitor of metalloproteinase 1 in the atria of wild-type (WT) and NPR-C$^{-/-}$ mice.

A, Right atrial (RA) *mmp2* mRNA expression in younger and older WT and NPR-C$^{-/-}$ mice (left) and as a function of frailty index (FI) score (right). *n*=19 for WT-younger, 20 for WT-older, 18 for NPR-C$^{-/-}$-younger, and 20 for NPR-C$^{-/-}$-older. **B**, Left atrial (LA) *mmp2* mRNA expression in younger and older WT and NPR-C$^{-/-}$ mice (left) and as a function of FI score (right). *n*=20 for WT-younger, 20 for WT-older, 19 for NPR-C$^{-/-}$-younger, and 20 for NPR-C$^{-/-}$-older. **C**, RA *mmp9* mRNA expression in younger and older WT and NPR-C$^{-/-}$ mice (left) and as a function of FI score (right). *n*=19 for WT-younger, 20 for WT-older, 20 for NPR-C$^{-/-}$-younger, and 19 for NPR-C$^{-/-}$-older. **D**, LA *mmp9* mRNA expression in younger and older WT and NPR-C$^{-/-}$ mice (left) and as a function of FI score (right). *n*=20 for WT-younger, 20 for WT-older, 20 for NPR-C$^{-/-}$-younger, and 20 for NPR-C$^{-/-}$-older. **E**, RA *timp1* mRNA expression in younger and older WT and NPR-C$^{-/-}$ mice (left) and as a function of FI score (right). *n*=17 for WT-younger, 20 for WT-older, 20 for NPR-C$^{-/-}$-younger, and 18 for NPR-C$^{-/-}$-older. **F**, LA *timp1* mRNA expression in younger and older WT and NPR-C$^{-/-}$ mice (left panel) and as a function of FI score (right panel). *n*=16 for WT-younger, 19 for WT-older, 19 for NPR-C$^{-/-}$-younger, and 20 for NPR-C$^{-/-}$-older. For figures as a function of chronological age *P<0.05 vs younger; +P<0.05 vs WT by 2-way ANOVA with a Tukey posthoc test. For figures as a function of FI score linear regressions analyzed using Pearson correlation.

quantifies overall health status by assessing general indicators of health across several organ systems.[7–9] Importantly, the specific items measured are not critical. Rather, the FI approach depends on having a minimum number of items in the index (≈30 items). As long as these items are associated with health status, increase in prevalence with aging, and cover a range of organ systems, the FI index will very accurately determine overall health status.[6,21,22] The mouse clinical FI meets all of these criteria.[7] FI score is strongly associated with health status and risk of death.[4,6] Thus, NPR-C$^{-/-}$ mice exhibit shortened lifespan in association with an overall decline in health status because of more rapid aging and early death.

Aging and frailty are highly associated with atrial dysfunction and AF development.[9,23] NPR-C has also been clearly linked to atrial dysfunction and AF susceptibility.[15,16,24] Accordingly, the links between NPR-C and frailty, and their impact on atrial arrhythmogenesis, were investigated in aging and frail NPR-C$^{-/-}$ mice where it was found that frailty is a strong predictor of AF burden as a function of health status including in a genetic model of shortened lifespan and accelerated aging because of loss of NPR-C.

Increased AF susceptibility in aging WT and NPR-C$^{-/-}$ mice was associated with impaired atrial electrical conduction. There was substantial variability in P wave duration and RA and LA conduction velocity across all groups, but especially in the older mice. As a result, there were no detectable differences in P wave duration or LA conduction velocity between older and younger NPR-C$^{-/-}$ mice. Similarly, conduction velocity differences were not detected in older NPR-C$^{-/-}$ mice and older WT mice. In contrast, frailty analysis showed that P wave duration as well as RA and LA conduction velocity, were strongly correlated with FI score. This indicates that these measures of atrial conduction are importantly affected by overall health status and that FI scores accurately predict P wave duration and atrial conduction velocity regardless of age or genotype. Impairments in atrial conduction can create a substrate for AF by shortening the wavelength for electrical reentry.[3,20] Age and NPR-C both contribute to this phenomenon and frailty can account for variability and identify differences that are not always apparent when studying distinct age groups.

Conduction velocity is determined in part by the Na^+ current.[20] Expression of *scn5a* mRNA (which encodes $Na_V1.5$) was reduced as a function of FI score in the left atrium (but not the right atrium). This is consistent with studies showing the left atrium is often an important site for AF initiation and suggests that changes in Na^+ current could contribute importantly to impairments in atrial conduction during the development of frailty. The basis for these changes in *scn5a* expression are not currently known and should be investigated in future studies.

Atrial APD was reduced in older WT and NPR-C$^{-/-}$ mice compared with younger mice, but not different between NPR-C$^{-/-}$ mice and WT mice within age groups, which is consistent with previous studies in young NPR-C$^{-/-}$ mice.[15] Once again, there was variability in all groups. Frailty analysis demonstrates that right and left APDs were also correlated with FI score; however, these correlations were not as strong as for P wave duration or conduction velocity, which may be because atrial APD is not affected by NPR-C ablation. Nevertheless, frailty analysis could still account for variability in age groups and atrial APD showed a clear relationship with FI score. Electrical reentry is more likely to occur when the refractory period is shorter, which occurs when atrial APD is reduced.[3,20] Thus, shortening of atrial APD with increasing frailty could partially explain the increase in AF susceptibility in more frail mice. Consistent with this, estimates of wavelength of reentry in optical mapping studies demonstrate that wavelength was strongly negatively correlated with FI score in the right and left atria.

NPR-C has been shown to modulate atrial conduction and arrhythmogenesis by affecting atrial fibrosis.[15] Aging also leads to atrial fibrosis.[9] Consistent with this, the present study demonstrates that fibrosis is increased with age and as a result of loss of NPR-C, with the highest atrial interstitial fibrosis levels observed in the left atrium of older NPR-C$^{-/-}$ mice. In addition, RA and LA fibrosis was strongly correlated with FI score indicating that health status has a large impact on atrial fibrosis and that frailty can effectively discriminate differences in atrial fibrosis regardless of age and genotype. Atrial fibrosis can be a critical determinant of impaired electrical conduction, shortening of wavelength of reentry, and AF occurrence.[3,20]

The expression of genes involved in collagen deposition and regulation identified increases in TIMP1 in the right and left atria of aged WT and NPR-C$^{-/-}$ mice. More importantly, frailty analysis revealed consistent correlations between TIMP1 expression and FI score in both atria. TIMP1 can enhance collagen deposition independently of its inhibitory effect on MMPs.[25] In addition, the ability of TIMP1 to inhibit MMPs could also lead to a change in the balance between MMP and TIMP activity that could result in collagen retention in the extracellular matrix.[26] Consistent with the latter concept, the ratios of TIMP1/MMP2 expression in the left atrium and TIMP1/MMP9 expression in both atria were also positively correlated with FI score.

Frailty analysis revealed some additional gene expression changes, including in TGFβ, MMP2, TIMP3, and TIMP4. An increase in TGFβ expression could contribute to enhanced collagen production[27] and alterations in MMP2, TIMP3, and/or TIMP4 expression could further contribute to a change in proteolytic degradation of collagens once deposited in the extracellular matrix.[26] However, changes in expression of these genes was not consistent across both atria. More studies are needed to determine the relative importance

of these changes in gene expression in mediating the development of atrial fibrosis.

AF susceptibility and the substrate for arrhythmia are importantly affected by the endocrine regulation of the atria.[24] NPs are potent regulators of atrial structure and function.[11,12] The findings in the present study demonstrate that disruption of normal NP signaling via NPR-C can contribute importantly to aging-dependent increases in frailty and that these changes in overall health status critically affect atrial electrophysiology. This indicates an essential role for NPs, acting in part via NPR-C, in maintaining cardiovascular health during the aging process. These findings suggest that NPR-C could be targeted to slow or prevent the development of frailty as well as atrial structure (ie, fibrosis) and function, which could lead to a reduction in AF susceptibility. Thus, the effects of NPR-C activation on frailty and AF susceptibility will be important to investigate in future studies. Mice heterozygous for NPR-C deletion (NPR-C$^{+/-}$) were not examined in the present study; however, previous studies have shown that younger NPR-C$^{+/-}$ mice are indistinguishable from WT mice[28] suggesting that NPR-C$^{+/-}$ mice would exhibit similar outcomes to WT mice during aging.

In summary, our study demonstrates an essential role for NPR-C in aging-dependent changes in health status (frailty) as well as atrial structure, function, and arrhythmogenesis. We also demonstrate that frailty analysis enables the accurate determination of health status across all ages and genotypes and that changes in atrial function are strongly correlated with FI score. Heterogeneity in aging represents a major challenge for understanding the pathogenesis of AF and for treating AF in aging patients. Our study demonstrates that frailty assessment is a powerful tool for dealing with this heterogeneity and that frailty can accurately predict atrial function and arrhythmogenesis during the aging process independently of chronological age, including in the setting of genetic alterations that alter longevity such as loss of NPR-C. Our study indicates that the NP system and NPR-C should be considered as novel targets for improving health status and preventing atrial arrhythmias in aging and frail populations.

ARTICLE INFORMATION

Received April 14, 2021; accepted August 17, 2021.

Affiliations

Department of Cardiac Sciences, Department of Physiology and Pharmacology, Libin Cardiovascular Institute, Cumming School of Medicine, University of Calgary, Alberta, Canada (H.J.J., M.M., R.A.R.). Department of Physiology and Biophysics, Faculty of Medicine, Dalhousie University, Halifax, Nova Scotia, Canada (S.A.R.).

Sources of Funding

This work was supported by The Heart and Stroke Foundation of Canada (G-18-0022148) and The Canadian Institutes of Health Research (PJT 166105 and MOP 142486) to Dr Rose. Dr Jansen was supported by a Killam Postdoctoral Fellowship and a Libin Cardiovascular Institute Postdoctoral Fellowship.

Disclosures

None.

Supplemental Materials

Supplemental Methods
Supplemental Table I
Supplemental Figures I–VIII

REFERENCES

1. Kornej J, Börschel CS, Benjamin EJ, Schnabel RB. Epidemiology of atrial fibrillation in the 21st century: novel methods and new insights. *Circ Res*. 2020;127:4–20. doi: 10.1161/CIRCRESAHA.120.316340
2. Chiang CE, Naditch-Brûlé L, Murin J, Goethals M, Inoue H, O'Neill J, Silva-Cardoso J, Zharinov O, Gamra H, Alam S, et al. Distribution and risk profile of paroxysmal, persistent, and permanent atrial fibrillation in routine clinical practice: insight from the real-life global survey evaluating patients with atrial fibrillation international registry. *Circ Arrhythm Electrophysiol*. 2012;5:632–639. doi: 10.1161/CIRCEP.112.970749
3. Heijman J, Voigt N, Nattel S, Dobrev D. Cellular and molecular electrophysiology of atrial fibrillation initiation, maintenance, and progression. *Circ Res*. 2014;114:1483–1499. doi: 10.1161/CIRCRESAHA.114.302226
4. Rockwood K, Blodgett JM, Theou O, Sun MH, Feridooni HA, Mitnitski A, Rose RA, Godin J, Gregson E, Howlett SE. A frailty index based on deficit accumulation quantifies mortality risk in humans and in mice. *Sci Rep*. 2017;7:43068. doi: 10.1038/srep43068
5. Guo Q, Du X, Ma CS. Atrial fibrillation and frailty. *J Geriatr Cardiol*. 2020;17:105–109. doi: 10.11909/j.issn.1671-5411.2020.02.007
6. Searle SD, Mitnitski A, Gahbauer EA, Gill TM, Rockwood K. A standard procedure for creating a frailty index. *BMC Geriatr*. 2008;8:24. doi: 10.1186/1471-2318-8-24
7. Whitehead JC, Hildebrand BA, Sun M, Rockwood MR, Rose RA, Rockwood K, Howlett SE. A clinical frailty index in aging mice: comparisons with frailty index data in humans. *J Gerontol A Biol Sci Med Sci*. 2014;69:621–632. doi: 10.1093/gerona/glt136
8. Moghtadaei M, Jansen HJ, Mackasey M, Rafferty SA, Bogachev O, Sapp JL, Howlett SE, Rose RA. The impacts of age and frailty on heart rate and sinoatrial node function. *J Physiol*. 2016;594:7105–7126. doi: 10.1113/JP272979
9. Jansen HJ, Moghtadaei M, Mackasey M, Rafferty SA, Bogachev O, Sapp JL, Howlett SE, Rose RA. Atrial structure, function and arrhythmogenesis in aged and frail mice. *Sci Rep*. 2017;7:44336. doi: 10.1038/srep44336
10. Feridooni HA, Kane AE, Ayaz O, Boroumandi A, Polidovitch N, Tsushima RG, Rose RA, Howlett SE. The impact of age and frailty on ventricular structure and function in C57BL/6J mice. *J Physiol*. 2017;595:3721–3742. doi: 10.1113/JP274134
11. Rose RA, Giles WR. Natriuretic peptide C receptor signalling in the heart and vasculature. *J Physiol*. 2008;586:353–366. doi: 10.1113/jphysiol.2007.144253
12. Moghtadaei M, Polina I, Rose RA. Electrophysiological effects of natriuretic peptides in the heart are mediated by multiple receptor subtypes. *Prog Biophys Mol Biol*. 2016;120:37–49. doi: 10.1016/j.pbiomolbio.2015.12.001
13. Sangaralingham SJ, Huntley BK, Martin FL, McKie PM, Bellavia D, Ichiki T, Harders GE, Chen HH, Burnett JC Jr. The aging heart, myocardial fibrosis, and its relationship to circulating C-type natriuretic peptide. *Hypertension*. 2011;57:201–207. doi: 10.1161/HYPERTENSIONAHA.110.160796
14. Sangaralingham SJ, Wang BH, Huang L, Kumfu S, Ichiki T, Krum H, Burnett JC Jr. Cardiorenal fibrosis and dysfunction in aging: imbalance in mediators and regulators of collagen. *Peptides*. 2016;76:108–114. doi: 10.1016/j.peptides.2016.01.004
15. Egom EE, Vella K, Hua R, Jansen HJ, Moghtadaei M, Polina I, Bogachev O, Hurnik R, Mackasey M, Rafferty S, et al. Impaired sinoatrial node function and increased susceptibility to atrial fibrillation in mice lacking natriuretic peptide receptor C. *J Physiol*. 2015;593:1127–1146. doi: 10.1113/jphysiol.2014.283135
16. Jansen HJ, Mackasey M, Moghtadaei M, Liu Y, Kaur J, Egom EE, Tuomi JM, Rafferty SA, Kirkby AW, Rose RA. NPR-C (Natriuretic Peptide Receptor-C) modulates the progression of angiotensin II-mediated atrial fibrillation and atrial remodeling in mice. *Circ Arrhythm Electrophysiol*. 2019;12:e006863. doi: 10.1161/CIRCEP.118.006863
17. Azer J, Hua R, Krishnaswamy PS, Rose RA. Effects of natriuretic peptides on electrical conduction in the sinoatrial node and atrial myocardium of the heart. *J Physiol*. 2014;592:1025–1045. doi: 10.1113/jphysiol.2013.265405

18. Jansen HJ, Mackasey M, Moghtadaei M, Belke DD, Egom EE, Tuomi JM, Rafferty SA, Kirkby AW, Rose RA. Distinct patterns of atrial electrical and structural remodeling in angiotensin II mediated atrial fibrillation. *J Mol Cell Cardiol*. 2018;124:12–25. doi: 10.1016/j.yjmcc.2018.09.011
19. Bohne LJ, Jansen HJ, Daniel I, Dorey TW, Moghtadaei M, Belke DD, Ezeani M, Rose RA. Electrical and structural remodeling contribute to atrial fibrillation in type 2 diabetic db/db mice. *Heart Rhythm*. 2021;18:118–129. doi: 10.1016/j.hrthm.2020.08.019
20. Jansen HJ, Bohne LJ, Gillis AM, Rose RA. Atrial remodeling and atrial fibrillation in acquired forms of cardiovascular disease. *Heart Rhythm O2*. 2020;1:147–159. doi: 10.1016/j.hroo.2020.05.002
21. Rockwood K, Mitnitski A. Frailty in relation to the accumulation of deficits. *J Gerontol A Biol Sci Med Sci*. 2007;62:722–727. doi: 10.1093/gerona/62.7.722
22. Rockwood K, Mitnitski A. Frailty defined by deficit accumulation and geriatric medicine defined by frailty. *Clin Geriatr Med*. 2011;27:17–26. doi: 10.1016/j.cger.2010.08.008
23. Villani ER, Tummolo AM, Palmer K, Gravina EM, Vetrano DL, Bernabei R, Onder G, Acampora N. Frailty and atrial fibrillation: a systematic review. *Eur J Intern Med*. 2018;56:33–38. doi: 10.1016/j.ejim.2018.04.018
24. Aguilar M, Rose RA, Takawale A, Nattel S, Reilly S. New aspects of endocrine control of atrial fibrillation and possibilities for clinical translation. *Cardiovasc Res*. 2021;117:1645–1661. doi: 10.1093/cvr/cvab080
25. Takawale A, Zhang P, Patel VB, Wang X, Oudit G, Kassiri Z. Tissue Inhibitor of Matrix Metalloproteinase-1 Promotes Myocardial Fibrosis by Mediating CD63-Integrin β1 Interaction. *Hypertension*. 2017;69:1092–1103. doi: 10.1161/HYPERTENSIONAHA.117.09045
26. Takawale A, Sakamuri SS, Kassiri Z. Extracellular matrix communication and turnover in cardiac physiology and pathology. *Compr Physiol*. 2015;5:687–719. doi: 10.1002/cphy.c140045
27. Leask A. Getting to the heart of the matter: new insights into cardiac fibrosis. *Circ Res*. 2015;116:1269–1276. doi: 10.1161/CIRCRESAHA.116.305381
28. Matsukawa N, Grzesik WJ, Takahashi N, Pandey KN, Pang S, Yamauchi M, Smithies O. The natriuretic peptide clearance receptor locally modulates the physiological effects of the natriuretic peptide system. *Proc Natl Acad Sci USA*. 1999;96:7403–7408. doi: 10.1073/pnas.96.13.7403

Supplemental Material

Supplemental Methods

Frailty assessment

Frailty was assessed in all mice using our non-invasive 31 item frailty index. Specific assessments of the integument, musculoskeletal, vestibulocochlear/auditory, ocular, nasal, digestive, urogenital and respiratory systems were performed. Signs of discomfort, body temperature and body mass were also assessed. All 31 items are listed in Figure I in the Data Supplement. Each item was given a score of 0 (no sign of deficit), 0.5 (mild deficit) or 1 (severe deficit). Deficits in body temperature and body mass were scored based on deviation from the mean in young and aged mice. The scores for each item were added together and the sum was divided by the number of items measured (i.e. 31 items) to provide an FI score between 0 (least frail) and 1 (most frail).

In vivo electrophysiology

A 1.2 French octapolar electrophysiology catheter containing 8 electrodes spaced 0.5 mm apart was used for intracardiac pacing experiments. Inducibility of AF was studied using burst pacing in the right atrium. We used 5 trains of burst pacing as follows: the first 2 s burst was given at a cycle length of 40 ms with a pulse duration of 5 ms. Following 2 min of stabilization a second 2 s burst was applied at a cycle length 20 ms with a pulse duration of 5 ms. After another 2 min of stabilization the final 2 s burst was given at a cycle length of 20 ms with a pulse duration of 10 ms. This was followed by 2 min of stabilization and then 100 beat bursts at cycle lengths of 25 and 20 ms with 2 min of stabilization between each. AF was defined as a rapid and irregular atrial rhythm (fibrillatory baseline in the ECG) with irregular RR

intervals lasting at least 1 s on the surface ECG. AERP measurements were determined using a S1-S2 protocol where an 8 stimulus drive train (S1) at a fixed cycle length of 100 ms was delivered followed by an extra stimulus (S2) at a progressively shorter cycle length. AERP was defined as the shortest S1-S2 interval that allowed for capture of the region of interest, defined as the P wave for AERP measurements. All ECG data were acquired using a Gould ACQ-7700 amplifier and Ponemah Physiology Platform software (Data Sciences International). Body temperature was maintained at 37˚C using a heating pad.

High-resolution optical mapping

High resolution optical mapping was used to study patterns of electrical conduction in the mouse atria. To isolate atrial preparations, mice were anesthetized by isoflurane inhalation and sacrificed by cervical dislocation. Hearts were excised into Krebs solution (37°C) containing (in mM): 118 NaCl, 4.7 KCl, 1.2 KH_2PO_4, 25 $NaHCO_3$, 1 $CaCl_2$, 1 $MgCl_2$, 11 glucose and bubbled with 95% O_2/5% CO_2 to maintain a pH of 7.4. The atria were dissected away from the ventricles and pinned in a dish with the endocardial surface facing upwards (towards the imaging equipment). The superior and inferior vena cavae were cut open so that the crista terminalis could be visualized, and the preparation could be pinned out flat with minimal tension.

The atrial preparation was superfused continuously with Krebs solution (37°C) bubbled with 95% O_2/5% CO_2 and allowed to equilibrate for ~10 min. The preparation was then incubated with the voltage sensitive dye RH-237 (15 µM; Biotium) for 20 min without superfusion while being bubbled with 95% O_2/5% CO_2. After the dye incubation period, superfusion was resumed with blebbistatin (10 µM; Cayman Chemical Company) added to the superfusate to suppress contractile activity and prevent motion artifacts.[1] Experiments were performed in sinus rhythm so that the cycle length (i.e. beating rate) of the atrial preparation was free to change. RH-237-loaded atrial preparations were illuminated with light from the X-Cite Xylis Broad Spectrum LED Illumination System (Excelitas Technologies) and filtered with a

520/35 nm excitation filter (Semrock). Emitted fluorescence was separated by a dichroic mirror (560 nm cut-off; Semrock) and filtered by a 715 nm long-pass emissions filter (Andover Corp.). Recordings were captured using a high-speed CMOS camera (MiCAM03-N256, SciMedia). Data were captured from an optical field of view of 11 x 11 mm at a frame rate of 1000 frames/s using BrainVision software (BrainVision Inc.). The spatial resolution was 42.5 x 42.5 μM for each pixel. Magnification was constant in all experiments and no pixel binning was used.

All optical data were analyzed using custom software written in MATLAB® (Mathworks). Pseudocolor electrical activation maps were generated from measurements of activation time at individual pixels as defined by assessment of dF/dt_{max} and background fluorescence was subtracted in all cases. Local conduction velocity (CV) was quantified specifically in the right atrial myocardium (within the right atrial appendage) and the left atrial myocardium (within the left atrial appendage). Activation times at each pixel from a 7 x 7 pixel array were determined and fit to a plane using the least squares fit method. The direction on this plane that is increasing the fastest represents the direction that is perpendicular to the wavefront of electrical propagation and the maximum slope represents the inverse of the speed of conduction in that direction. With a spatial resolution of 42.5 x 42.5 μM per pixel, the area of the 7 x 7 pixel array was 297.5 x 297.5 μM. This approach allows assessment the maximum local CV vectors in the atrial region of interest. Optical APs were assessed by measuring the change in fluorescence as a function of time at individual pixels within the right and left atria.

Histology

Interstitial collagen was assessed by picrosirius red staining of paraffin-embedded sections (5 μM) through the right and left atria. Fast green was used to counterstain the myocardium. Fibrosis was quantified using ImageJ software.

Quantitative PCR

Quantitative gene expression was measured in the right and left atria. Intron spanning primers were designed for *scn5a* ($Na_V1.5$), *col1a* (collagen type I), *col3a* (collagen type III), *tgfb1* (transforming growth factor β), *mmp2* (matrix metalloproteinase 2), *mmp9* (matrix metalloproteinase 9), *timp1* (tissue inhibitor of metalloproteinase 1), *timp2* (tissue inhibitor of metalloproteinase 2), *timp3* (tissue inhibitor of metalloproteinase 3), *timp4* (tissue inhibitor of metalloproteinase 4) and glyceraldehyde 3-phosphate dehydrogenase (GAPDH) (reference gene) were used. GAPDH expression was confirmed to be stable among all experimental groups. Primer sequences are listed in Table I below.

Total RNA was isolated from right or left atrial appendages using a PureZOL™ RNA Isolation Reagent and the Aurum™ Total RNA Fatty and Fibrous Tissue Kit (Bio-Rad Laboratories) as per kit instructions. RNA samples were eluted from the spin column in 40 µL elution buffer. RNA yield and purity were assessed using a Nanophotometer (Implen). All samples had a A_{260}/A_{280} of over 2.0 and therefore were free of DNA contamination. Next, cDNA (5 ng/µL) was synthesized using the iScript™ cDNA Synthesis Kit (Bio-Rad Laboratories). Reactions were performed in a Bio-Rad MyCycler thermal cycler using the following protocol: 5 min of priming at 25ºC followed by reverse transcription for 30 min at 42ºC then 5 min at 85ºC to inactivate reverse transcriptase.

All qPCR reactions were run in duplicate in 10 µL reactions that contained the following: 4 µL sample cDNA, 5.6 µL GoTaq® qPCR Master Mix (Promega), and 0.4 µL primers. Primers were reconstituted to a final concentration of 100 µM with nuclease free water and stored at -20ºC until use. Primers were diluted to 10 µM for qPCR reactions. RT-qPCR reactions were performed using the CFX96 Touch™ Real-Time PCR Detection System (Bio-Rad) using the following protocol: Taq polymerase was activated for 2 min at 95ºC followed by 39 cycles of denaturing for 15 s at 95ºC, annealing for 30 s at 60ºC, and extension for 30s at 72ºC. This was followed by melt curve analysis from 65-95ºC in 0.5ºC increments. Data were analyzed using

the $2^{-\Delta\Delta C_T}$ method using the CFX Manager Software version 3.1 (Bio-Rad). Gene expression was normalized to GAPDH.

Table I: Quantitative qPCR primers

Gene	Gene product	Primer Sequence (5'→ 3')	Amplicon length
scn5a	$Na_v1.5$	Forward: GGAGTACGCCGACAAGATGT Reverse: ATCTCGGCAAAGCCTAAGGT	171
col1a	Collagen type I	Forward: GCGGACTCTGTTGCTGCTTGC Reverse: GACCTGCGGGACCCCTTTGT	125
col3a	Collagen type III	Forward: AGATCCGGGTCCTCCTGGCATTC Reverse: CTGGTCCCGGATAGCCACCCAT	194
tgfb1	TGFβ	CGAGGTGACCTGGGCACCATCCATGAC CTGCTCCACCTTGGGCTTGCGACCCAC	405
mmp2	MMP2	Forward: CCACGTGACAAGCCCATGGGGCCC Reverse: GCAGCCTAGCCAGTCGGATTTGATG	486
mmp9	MMP9	Forward: TCGCGTGGATAAGGAGTTCTC Reverse: ATGGCAGAAATAGGCTTTGTCTTG	82
timp1	TIMP1	Forward: CAGATACCATGATGGCCCCC Reverse: CGCTGGTATAAGGTGGTCTCG	190
timp2	TIMP2	Forward: CCAGAAGAAGAGCCTGAACCA Reverse: GTCCATCCAGAGGCACTCATC	112
timp3	TIMP3	Forward: GGCCTCAATTACCGCTACCA Reverse: CTGATAGCCAGGGTACCCAAAA	135
timp4	TIMP4	Forward: TGCAGAGGGAGAGCCTGAA Reverse: GGTACATGGCACTGCATAGCA	180
GAPDH	GAPDH	Forward: CACCCTTCAAGTGGGCCCCG Reverse: CACCCTTCAAGTGGGCCCCG	227

Supplemental Figures

Date: _____

Mouse #: _____ **Date of Birth:** _____ **Sex:** F M

Body weight (g): _____ **Body surface temperature (°C):** _____

Rating: 0 = absent 0.5 = mild 1 = severe

				NOTES:
Integument:				
❖ Alopecia	0	0.5	1	_____
❖ Loss of fur colour	0	0.5	1	_____
❖ Dermatitis	0	0.5	1	_____
❖ Loss of whiskers	0	0.5	1	_____
❖ Coat condition	0	0.5	1	_____
Physical/Musculoskeletal:				
❖ Tumours	0	0.5	1	_____
❖ Distended abdomen	0	0.5	1	_____
❖ Kyphosis	0	0.5	1	_____
❖ Tail stiffening	0	0.5	1	_____
❖ Gait disorders	0	0.5	1	_____
❖ Tremor	0	0.5	1	_____
❖ Forelimb grip strength	0	0.5	1	_____
❖ Body condition score	0	0.5	1	_____
Vestibulocochlear/Auditory:				
❖ Vestibular disturbance	0	0.5	1	_____
❖ Hearing loss	0	0.5	1	_____
Ocular/Nasal:				
❖ Cataracts	0	0.5	1	_____
❖ Corneal opacity	0	0.5	1	_____
❖ Eye discharge/swelling	0	0.5	1	_____
❖ Microphthalmia	0	0.5	1	_____
❖ Vision loss	0	0.5	1	_____
❖ Menace reflex	0	0.5	1	_____
❖ Nasal discharge	0	0.5	1	_____
Digestive/Urogenital:				
❖ Malocclusions	0	0.5	1	_____
❖ Rectal prolapse	0	0.5	1	_____
❖ Vaginal/uterine/penile prolapse	0	0.5	1	_____
❖ Diarrhoea	0	0.5	1	_____
Respiratory system:				
❖ Breathing rate/depth	0	0.5	1	_____
Discomfort:				
❖ Mouse Grimace Scale	0	0.5	1	_____
❖ Piloerection	0	0.5	1	_____
❖ **Temperature score:** _____				
❖ **Body weight score:** _____				

Total Score/ Max Score:

Figure I: Mouse frailty index assessment form.

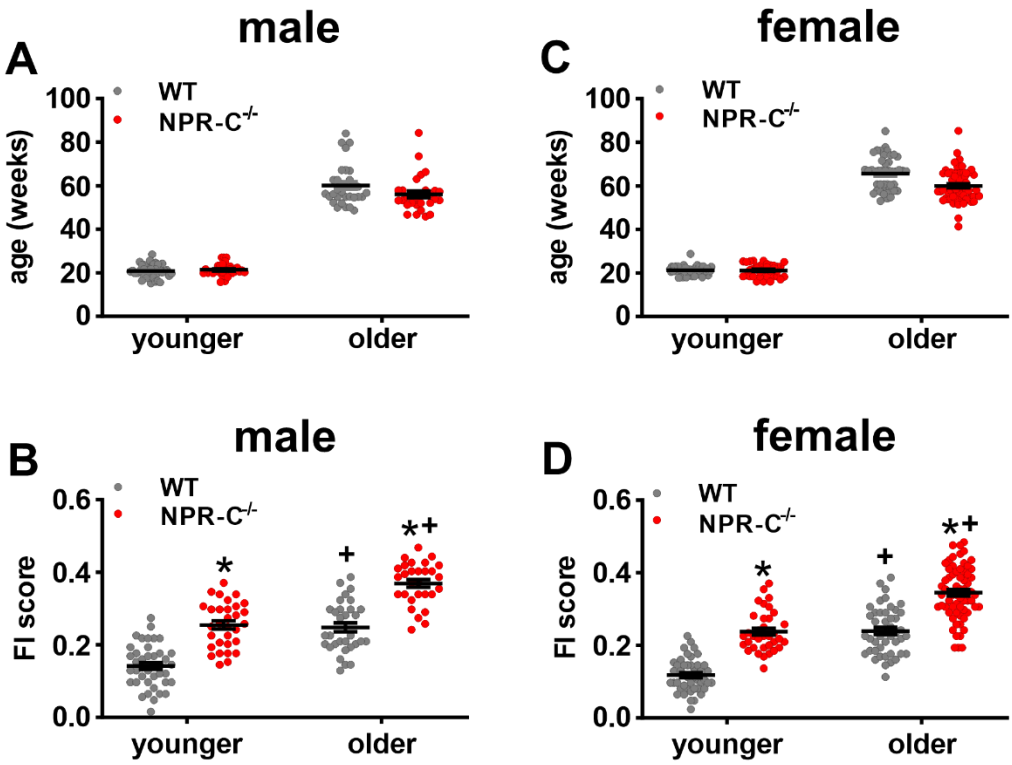

Figure II: Ages and frailty index scores for male and female WT and NPR-C$^{-/-}$ mice. A: Ages of male younger and older WT and NPR-C$^{-/-}$ mice used in this study. **B:** Frailty index (FI) scores in male younger and older WT and NPR-C$^{-/-}$ mice used in this study (same mice as panel A). For panels A and B *n*=41 for WT-younger, 31 for WT-older, 31 for NPR-C$^{-/-}$-younger and 29 for NPR-C$^{-/-}$-older. **C:** Ages of female younger and older WT and NPR-C$^{-/-}$ mice used in this study. **D:** Frailty index (FI) scores in female younger and older WT and NPR-C$^{-/-}$ mice used in this study (same mice as panel C). For panels C and D *n*=44 for WT-younger, 45 for WT-older, 35 for NPR-C$^{-/-}$-younger and 66 for NPR-C$^{-/-}$-older. *P<0.05 vs. WT; ^{+}P<0.05 vs. younger by two way ANOVA with a Tukey posthoc test.

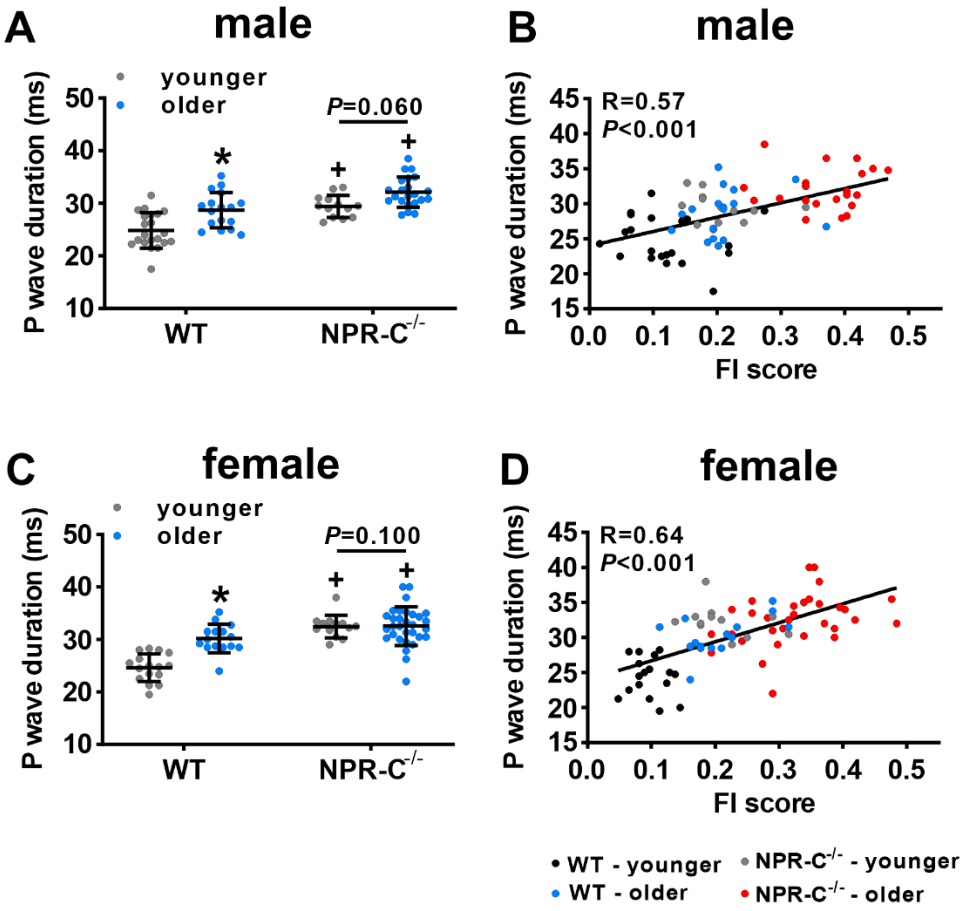

Figure III: P wave duration in male and female WT and NPR-C$^{-/-}$ mice. A: P wave duration in male younger and older WT and NPR-C$^{-/-}$ mice. *P<0.05 vs. younger; ^{+}P<0.05 vs. WT by two-way ANOVA with a Tukey posthoc test. **B:** P wave duration as a function of FI score for male younger and older WT and NPR-C$^{-/-}$ mice (same mice as panel A). Linear regression analyzed using Pearson's correlation. For panels A and B n=21 for WT-younger, 17 for WT-older, 13 for NPR-C$^{-/-}$-older and 32 for NPR-C$^{-/-}$-older. **C:** P wave duration in female younger and older WT and NPR-C$^{-/-}$ mice. *P<0.05 vs. younger; ^{+}P<0.05 vs. WT by two-way ANOVA with a Tukey posthoc test. **D:** P wave duration as a function of FI score for female younger and older WT and NPR-C$^{-/-}$ mice (same mice as panel C). Linear regression analyzed using Pearson's correlation. For panels C and D n=16 for WT-younger, 15 for WT-older, 13 for NPR-C$^{-/-}$-older and 31 for NPR-C$^{-/-}$-older.

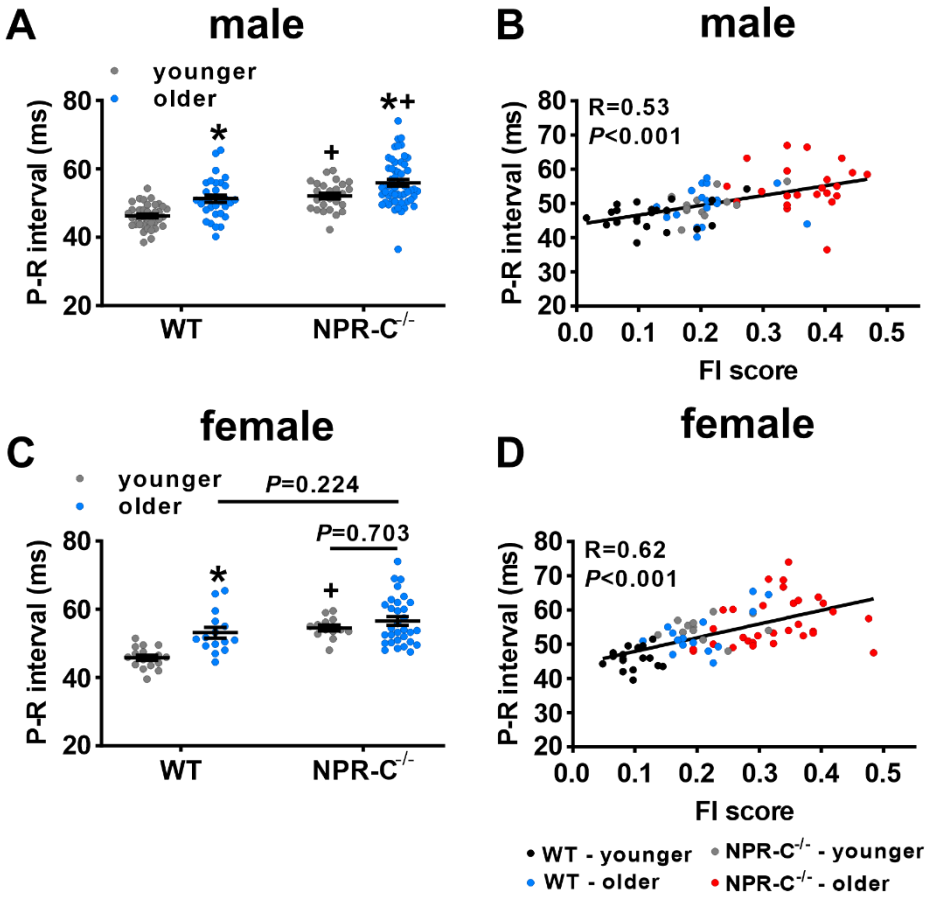

Figure IV: PR interval in male and female WT and NPR-C$^{-/-}$ mice. A: PR interval in male younger and older WT and NPR-C$^{-/-}$ mice. *P<0.05 vs. younger; ^{+}P<0.05 vs. WT by two-way ANOVA with a Tukey posthoc test. **B:** PR interval as a function of FI score for male younger and older WT and NPR-C$^{-/-}$ mice (same mice as panel A). Linear regression analyzed using Pearson's correlation. For panels A and B n=38 for WT-younger, 32 for WT-older, 26 for NPR-C$^{-/-}$-older and 53 for NPR-C$^{-/-}$-older. **C:** PR interval in female younger and older WT and NPR-C$^{-/-}$ mice. *P<0.05 vs. younger; ^{+}P<0.05 vs. WT by two-way ANOVA with a Tukey posthoc test. **D:** PR interval as a function of FI score for female younger and older WT and NPR-C$^{-/-}$ mice (same mice as panel C). Linear regression analyzed using Pearson's correlation. For panels C and D n=17 for WT-younger, 15 for WT-older, 13 for NPR-C$^{-/-}$-older and 31 for NPR-C$^{-/-}$-older.

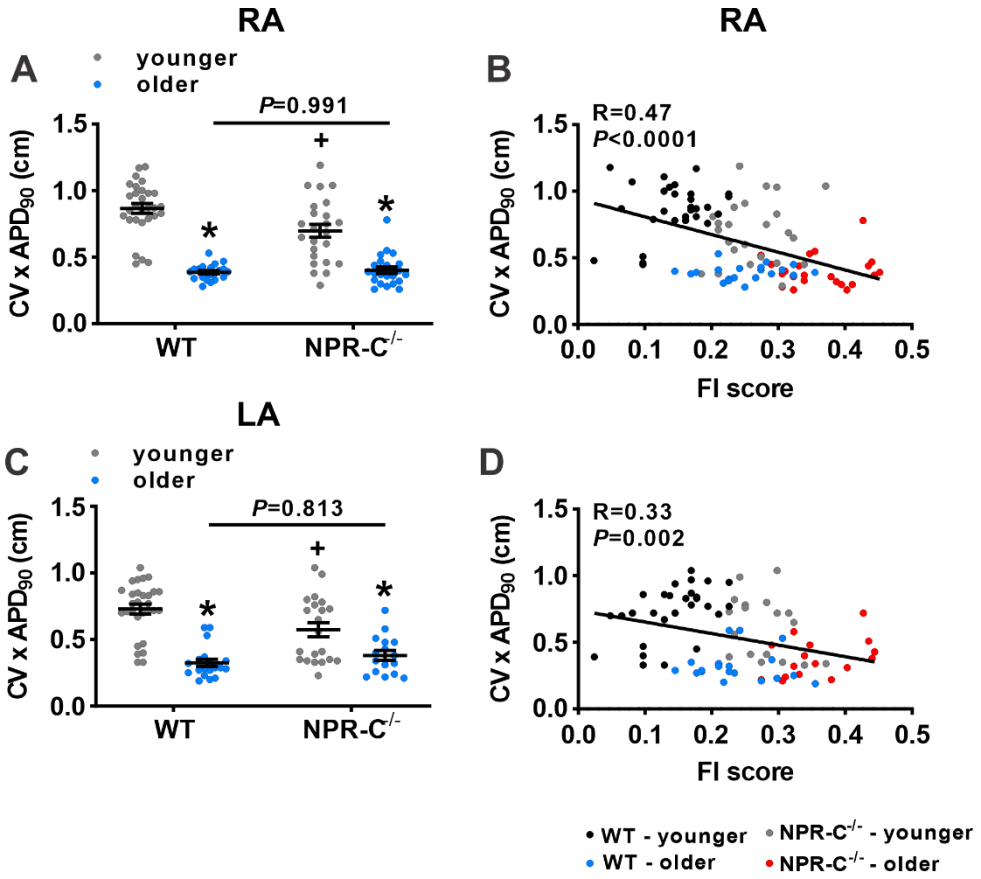

Figure V: Estimation of wavelength of re-entry in the atria of WT and NPR-C$^{-/-}$ mice. Wavelength was calculated as the product of conduction velocity and AP duration at 90% repolarization (APD_{90}). **A:** Right atrial wavelength in younger and older WT and NPR-C$^{-/-}$ mice. *n*=29 for WT-younger, 21 for WT-older, 24 for NPR-C$^{-/-}$-younger and 22 for NPR-C$^{-/-}$-older. **P*<0.05 vs. younger; $^{+}$*P*<0.05 vs. WT by two-way ANOVA with a Tukey posthoc test. **B:** Right atrial wavelength in younger and older WT and NPR-C$^{-/-}$ mice as a function of FI score (same mice as panel A). Linear regression analyzed using Pearson's correlation. **C:** Left atrial wavelength in younger and older WT and NPR-C$^{-/-}$ mice. *n*=29 for WT-younger, 19 for WT-older, 21 for NPR-C$^{-/-}$-younger and 16 for NPR-C$^{-/-}$-older. **P*<0.05 vs. younger; $^{+}$*P*<0.05 vs. WT by two-way ANOVA with a Tukey posthoc test. **D:** Left atrial wavelength in younger and older WT and NPR-C$^{-/-}$ mice as a function of FI score (same mice as panel C). Linear regression analyzed using Pearson's correlation.

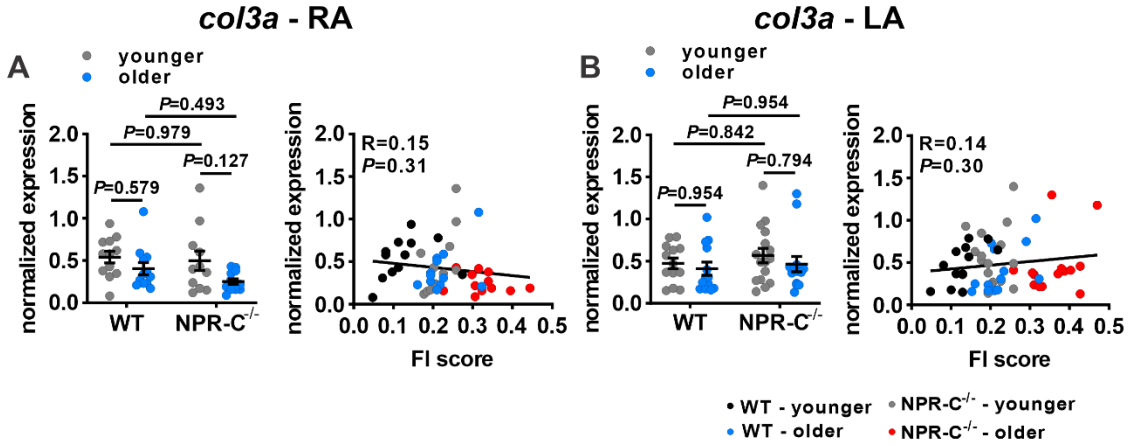

Figure VI: Expression of collagen type III in the atrial of WT and NPR-C$^{-/-}$ mice. A: Right atrial (RA) *col3a* mRNA expression in younger and older WT and NPR-C$^{-/-}$ mice (left panel) and as a function of FI score (right panel). *n*=12 for WT-younger, 12 for WT-older, 11 for NPR-C$^{-/-}$-younger and 12 for NPR-C$^{-/-}$-older. **B:** Left atrial (LA) *col3a* mRNA expression in younger and older WT and NPR-C$^{-/-}$ mice (left panel) and as a function of FI score (right panel). *n*=13 for WT-younger, 13 for WT-older, 16 for NPR-C$^{-/-}$-younger and 14 for NPR-C$^{-/-}$-older. For figures as a function of chronological age **P*<0.05 vs. younger; $^{+}$*P*<0.05 vs. WT by two-way ANOVA with a Tukey posthoc test. For figures as a function of FI score linear regressions analyzed using Pearson's correlation.

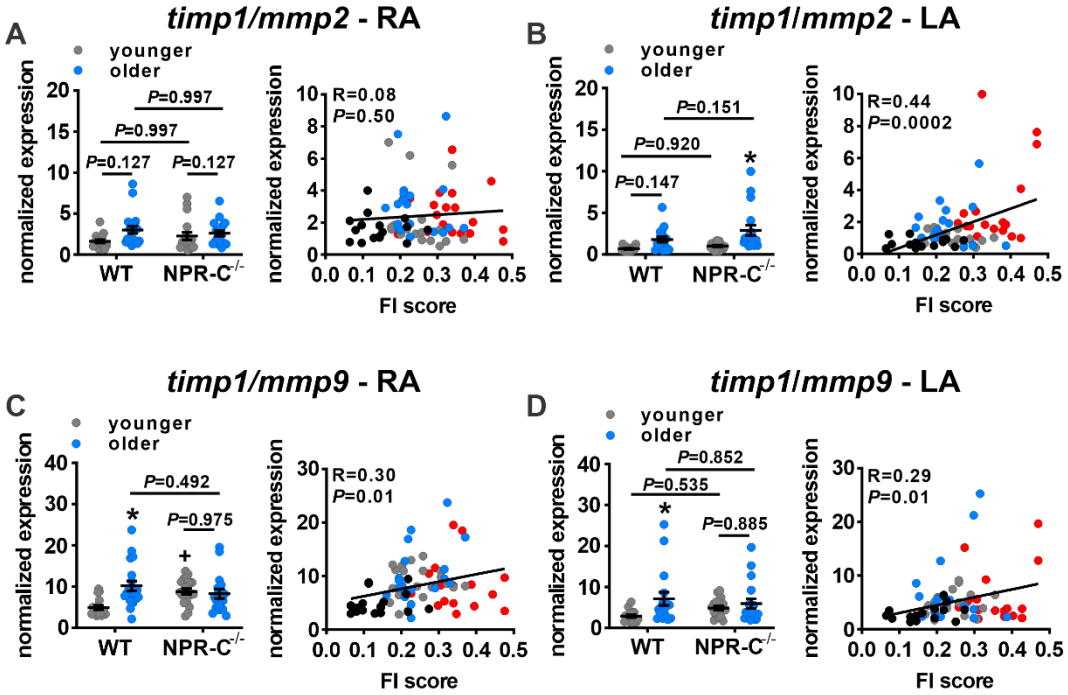

Figure VII: Ratio of expression of TIMP1 and MMPs in the atria of WT and NPR-C$^{-/-}$ mice. **A:** Right atrial (RA) ratio of *timp1/mmp2* in younger and older WT and NPR-C$^{-/-}$ mice (left panel) and as a function of FI score (right panel). *n*=17 for WT-younger, 20 for WT-older, 18 for NPR-C$^{-/-}$-younger and 18 for NPR-C$^{-/-}$-older. **B:** Left atrial (RA) ratio of *timp1/mmp2* in younger and older WT and NPR-C$^{-/-}$ mice (left panel) and as a function of FI score (right panel). *n*=16 for WT-younger, 17 for WT-older, 18 for NPR-C$^{-/-}$-younger and 18 for NPR-C$^{-/-}$-older. **C:** Right atrial (RA) ratio of *timp1/mmp9* in younger and older WT and NPR-C$^{-/-}$ mice (left panel) and as a function of FI score (right panel). *n*=17 for WT-younger, 20 for WT-older, 17 for NPR-C$^{-/-}$-younger and 20 for NPR-C$^{-/-}$-older. **D:** Left atrial (RA) ratio of *timp1/mmp9* in younger and older WT and NPR-C$^{-/-}$ mice (left panel) and as a function of FI score (right panel). *n*=16 for WT-younger, 17 for WT-older, 19 for NPR-C$^{-/-}$-younger and 18 for NPR-C$^{-/-}$-older. For figures as a function of chronological age **P*<0.05 vs. younger; $^{+}$*P*<0.05 vs. WT by two-way ANOVA with a Tukey posthoc test. For figures as a function of FI score linear regressions analyzed using Pearson's correlation.

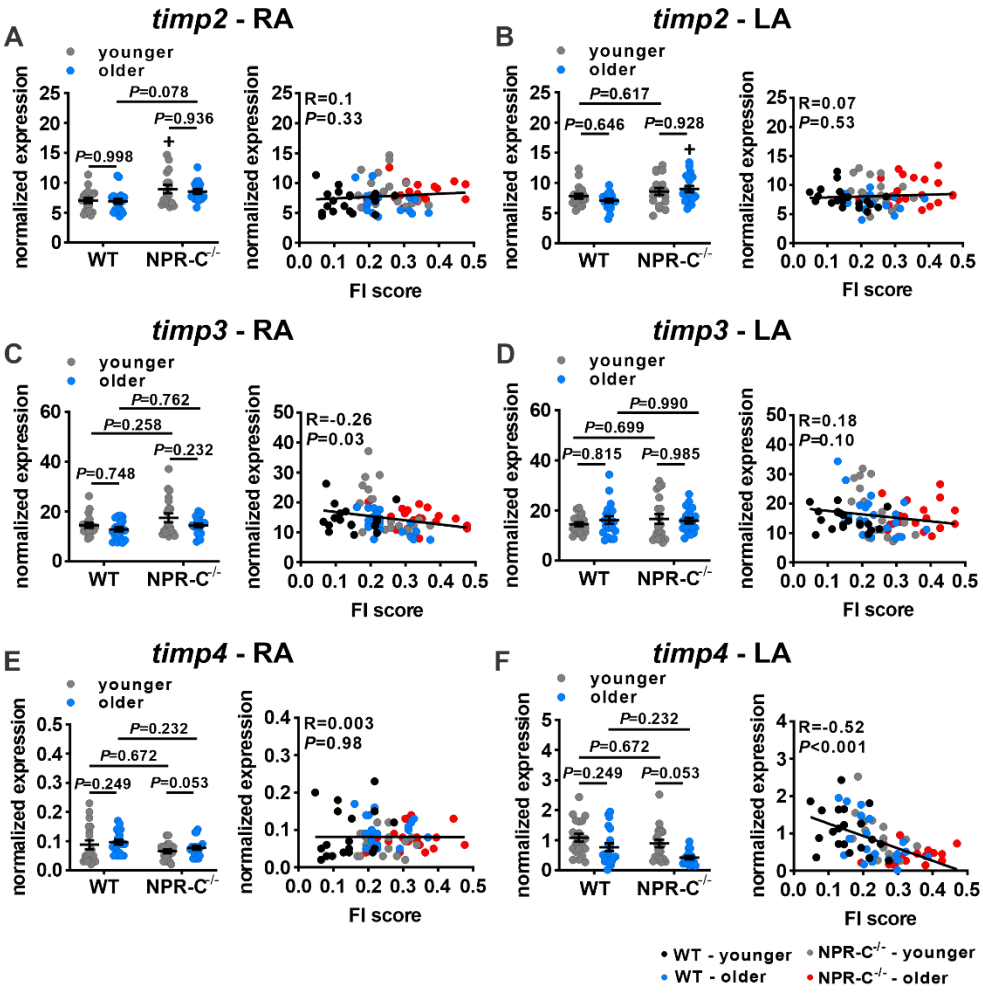

Figure VIII: Expression of tissue inhibitors of metalloproteinase 2, 3 and 4 in the atria of WT and NPR-C$^{-/-}$ mice. A: Right atrial (RA) *timp2* mRNA expression in younger and older WT and NPR-C$^{-/-}$ mice (left panel) and as a function of FI score (right panel). *n*=19 for WT-younger, 20 for WT-older, 17 for NPR-C$^{-/-}$-younger and 18 for NPR-C$^{-/-}$-older. **B:** Left atrial (LA) *timp2* mRNA expression in younger and older WT and NPR-C$^{-/-}$ mice (left panel) and as a function of FI score (right panel). *n*=20 for WT-younger, 18 for WT-older, 18 for NPR-C$^{-/-}$-younger and 20 for NPR-C$^{-/-}$-older. **C:** Right atrial (RA) *timp3* mRNA expression in younger and older WT and NPR-C$^{-/-}$ mice (left panel) and as a function of FI score (right panel). *n*=19 for WT-younger, 20 for WT-older, 20 for NPR-C$^{-/-}$-younger and 20 for NPR-C$^{-/-}$-older. **D:** Left atrial (LA) *timp3* mRNA expression in younger and older WT and NPR-C$^{-/-}$ mice (left panel) and as a function of FI score (right panel). *n*=20 for WT-younger, 20 for WT-older, 19 for NPR-C$^{-/-}$-younger and 19 for NPR-C$^{-/-}$-older. **E:** Right atrial (RA) *timp4* mRNA expression in younger and older WT and NPR-C$^{-/-}$ mice (left panel) and as a function of FI score (right panel). *n*=19 for WT-younger, 20 for WT-older, 20 for NPR-C$^{-/-}$-younger and 19 for NPR-C$^{-/-}$-older. **F:** Left atrial (LA) *timp4* mRNA expression in younger and older WT and NPR-C$^{-/-}$ mice (left panel) and as a function of FI score (right panel). *n*=20 for WT-younger, 20 for WT-older, 20 for NPR-C$^{-/-}$-younger and 16 for NPR-C$^{-/-}$-older. For figures as a function of chronological age **P*<0.05 vs. younger; $^{+}$*P*<0.05 vs. WT by two-way ANOVA with a Tukey posthoc test. For figures as a function of FI score linear regressions analyzed using Pearson's correlation.